Regulation of retinal axonal projections by the R3 receptor-like protein tyrosine phosphatase subfamily in mice

Yu, Yang

Doctor of Philosophy

Department of Basic Biology
School of Life Science
SOKENDAI (The Graduate University for Advanced Studies)

Table of contents

List of figures

Abbreviations

Abl	Abelson tyrosine kinase
Arg	Abl-related protein
CRD	cysteine-rich domain
DiI	1,1'-dioctadecyl-3,3,3'3'-tetramethylindocarbocyanine
dLGN	dorsal lateral geniculate nucleus ()
DKO	*Ptpro*/*Ptprj* double-deficient mice
EC	endothelial cells
FBS	fetal bovine serum
FN	fibronectin type III repeats
INL	inner nuclear layer
NRTKs	non-receptor tyrosine kinases
OC	optic chiasm
pAbl	phosphorylated c-Abl
PBM	PDZ binding motif
PTP	protein tyrosine phosphatases
PTPRJ	protein tyrosine phosphatases receptor type J
Ptprj-KO	*Ptprj*-deficient mice
PTPRO	protein tyrosine phosphatases receptor type O
Ptpro-KO	*Ptpro*-deficient mice
pTyr	phosphotyrosine
pEph	phosphorylated-Eph receptors
RGC	retinal ganglion cell
RPTP	receptor-like protein tyrosine phosphatase

RPTK	receptor-type protein tyrosine kinase
RT-qPCR	reverse transcription-quantitative PCR
SC	superior colliculus
TZ	terminal zone
WT	wild-type
SAM	sterile-α-motif

Abstract

Retinal ganglion cell (RGC) axons convey visual information from the eye to the brain through a long pathway, and the correct projection of their axons to the visual center is prerequisite for proper vision. RGC axons pass through the optic chiasm (OC), and then make terminal zones in the superior colliculus (SC). In mice, most axons cross the midline and project contralaterally, whereas a fraction of RGC axons from the ventrotemporal region avoid the midline of the OC and project ipsilaterally. In the SC, retinal axons establish the topographic map: nasal and temporal axons project to the posterior and anterior SC, respectively, while dorsal and ventral retinas are connected to the lateral and medial SC, respectively. Eph receptor protein tyrosine kinases and their ligands ephrins have been implicated in the retinal axonal projection through the OC and the establishment of topographic maps in the SC. Our laboratory previously demonstrated that PTPRO, a receptor-like protein tyrosine phosphatase (RPTP), controlled the projection of retinal axons though the regulation of Eph activities in chick. But it has not been elucidated which RPTPs regulate Eph activities in the retinal axons in mammals.

RPTPs are classified into eight subfamilies based on the sequence homology. The R3 RPTP subfamily, including PTPRB, PTPRH, PTPRJ and PTPRO, is characterized by extracellular fibronectin type III repeats, a transmembrane domain, and a single phosphatase domain in the intracellular regions. In this study, I investigated functional roles of R3 RPTPs in the mouse RGC axonal projection.

First, I examined mRNA expression of R3 RPTPs in the mouse retina, and I found that *Ptpro* and *Ptprj,* but not *Ptprb* or *Ptprh,* were expressed in the developing retina. The expression level of *Ptprj* was markedly higher than that of *Ptpro*. *In situ*

hybridization showed that both *Ptprj* and *Ptpro* were expressed in the ganglion cell layer and inner nuclear layer. To determine whether PTPRJ and PTPRO is implicated in the projection of retinal axons, I examined *Ptpro*-knockout (*Ptpro*-KO), *Ptprj*-KO, and *Ptpro*/*Ptprj* double-KO (DKO) mice. I found that phosphotyrosine levels of both EphA and EphB receptors were significantly upregulated in the *Ptprj*-KO and DKO retina, but not in the *Ptpro*-KO retina. To investigate the sensitivity of retinal axons to ephrins, I performed neurite extension assays using ephrinB2, and growth cone collapse assays using ephrinA2 and ephrinA5, and revealed that the sensitivity to these ephrins was significantly enhanced in retinal axons of *Ptprj*-KO and DKO mice.

Next, I examined the projection of retinal axons though the OC and topographic map formation in the SC in these mutant mice. *In vivo* axon tracing experiments revealed that the proportion of retinal axons that projected ipsilaterally or misrouted to the contralateral eye at the OC was increased in *Ptprj*-KO mice and DKO mice compared with WT mice. These results suggested that PTPRJ mainly controlled the guidance of retinal axons at the OC through the regulation of EphB signaling. In addition, nasal, ventral, and centrotemporal retinal axons of *Ptprj*-KO and DKO mice exhibited ectopic terminal zones anteriorly shifted in the SC. These results indicated that retinal axons of *Ptprj*-KO and DKO mice exhibited hyperactivity to ephrins. In all analyses, I detected no significant difference between WT and *Ptpro*-KO mice.

Eph signaling is reportedly mediated by c-Abl kinases in some cell types. I examined the activation of c-Abl after stimulation with ephrinB2 and A2 in dissociated retinal neurons and found that these ephrins induced the phosphorylation (activation) of c-Abl. Furthermore, neurite extension assays and growth cone collapse assays indicated that Eph repulsive signaling is partially mediated by c-Abl. I demonstrated that c-Abl was a substrate for PTPRO and PTPRJ. And I found that phosphorylation

levels of c-Abl in the *Ptprj*-KO and DKO retina, but not in the *Ptpro*-KO retina, were significantly higher compared with the WT retina. Forced activation of c-Abl kinases *in vivo* by a c-Abl activator induced similar abnormal retinal axonal projections observed in *Ptprj*-KO and DKO mice: when mice were treated with a c-Abl activator, the proportion of retinal axons that projected to the ipsilateral side or misrouted to the contralateral eye at the OC was increased, and nasal axons aberrantly terminated anterior to their topographically appropriate position of the SC. These results suggested that c-Abl kinases are required for the transduction of repulsive signals of Eph receptors in RGC axons, and that PTPRJ suppresses c-Abl activity as well as that of Eph receptors. Taken all together, I concluded that PTPRJ mainly regulates the projection of retinal axons through the suppression of Eph signaling by dephosphorylating both Eph and c-Abl kinases.

Introduction

General view of the visual system

Visual information is relayed from the eye to the brain along axons of retinal ganglion cells (RGCs). The retinal axons exit the eye at the optic disc and cross the midline at the optic chiasm (OC) to form the optic tract, and then extend to their targets: the dorsal lateral geniculate nucleus (dLGN) in the thalamus and the superior colliculus (SC) in the mid-brain in vertebrates (Fig. I.1). The correct axonal projection of retinal axons is a prerequisite for proper vision and vision-guided behaviors (Simon et al., 1992).

In mammals with binocular vision, retinal axons from each eye project either ipsilaterally or contralaterally through the OC (Marcus et al., 1996). The ipsilateral projection forms an overlapping field, which is considered to be necessary for acquiring high-quality binocular vision and stereopsis (Alais D, 1999; Jeffery, 2001). Thereafter, retinal axons establish a topographic map in the SC in order to generate a spatially matched projection of visual images to the brain: nasal and temporal axons project to the posterior and anterior SC, respectively, while dorsal and ventral retinas are connected to the lateral and medial SC, respectively.

During the topographic map formation of retinal axons, the proper axon guidance is thought to be controlled by the interactions between the receptors in retinal axons and their chemoattractive or repulsive ligands present along the pathway and in the target zone (Sperry, 1963; Chilton, 2006). Recent studies have identified a large number of guidance molecules and their receptors, such as ephrins/Ephs, BDNF/TrkB and Slit/Robo, which control the axon guidance of retinal axons at the OC and the formation of a topographic map in the visual system. (Cheng et al. 1995).

The molecular mechanism of the optic chiasm formation

In lower vertebrates such as chick and fish, neither ipsilaterally projecting axons nor binocular overlaps in the visual field are observed (Guillery, 1995; Jeffery, 2001). In mice, only 3 to 5% of retinal axons in the ventrotemporal (VT) region project ipsilaterally, while retinal axons outside this crescent region project contralaterally (Fig. I.2) (Mann and Holt, 2001; Petros et al., 2008). The repulsive ephrinB2-EphB1 interaction directs the ipsilateral retinal projection in mice: retinal axons from the VT portion express high levels of EphB1 receptors to sense ephrinB2 on the glial cells at the OC and turn ipsilaterally (Williams et al., 2003).

The molecular mechanisms of the retinocollicular map formation

In the topographic retinocollicular map, nasal retinal axons project to the posterior (P) SC, while temporal retinal axons map to the anterior (A) SC. Previous studies have proven that ephrinA/EphA signaling is critical in mapping the retinocollicular projection along the A-P axis (Brown et al., 2000; Wilkinson, 2000; Takahashi et al., 2003; McLaughlin and O'Leary, 2005; Sakuta et al., 2006; Takahashi et al., 2009) (Fig. I.3). In the mouse retina, EphA receptors are expressed in a decreasing gradient from the temporal to nasal retina, and ephrinAs are expressed in an increasing gradient from the anterior-posterior region in the SC (Connor et al., 1998). EphrinA-EphA repellant interactions between the SC and retinal axons prevent temporal axons strongly expressing EphA from invading the ephrinA-rich posterior region of the SC, while permit nasal axons weakly expressing EphA to enter and terminate in the posterior region (Marcus et al., 1996; Hornberger et al., 1999) (Fig. I.3).

On the other hand, ventral retinal axons project to the medial (M) SC, while dorsal retinal axons map to the lateral (L) SC. The EphB receptors and their membrane-bound ligands, ephrinBs are required for the topographic map formation along the M-

L axis of the SC (Hindges et al., 2002; McLaughlin et al., 2003a) (Fig. I.3). EphBs are expressed in a ventral high-dorsal low gradient in the retinas, while ephrinBs are expressed in a medial high-lateral low gradient in the SC in many vertebrates including mice (McLaughlin et al., 2003a; Hindges et al., 2002) (Fig. I.3). Therefore, the interactions between EphBs on ventral retinal axons and ephrinBs in the medial SC are considered not to be repulsive, but attractive (McLaughlin et al., 2003b). Previous studies analyzing retinocollicular projections in EphB-deficient mice have indicated that EphBs in ventral retinal axons are necessary for topographic map formation along the M-L axis in the SC (Hindges et al., 2002; Thakar et al., 2011).

Reversible protein tyrosine phosphorylation

Protein tyrosyl phosphorylation is one of the most common and important post-translational modifications. The tyrosine phosphorylation level of each protein is determined by the balance between actions of protein tyrosine kinases (PTKs) and protein tyrosine phosphatases (PTPs): proteins are phosphorylated on tyrosine residues by PTKs and dephosphorylated by PTPs. The reversible tyrosine phosphorylation regulates a number of biological processes, such as cell proliferation, differentiation, migration, axon navigation, metabolic homeostasis, and even in cancer development (Stoker et al., 2005; Johnson and van Vactor, 2003).

The protein tyrosine kinase and phosphatase families

Human genome contains 91 PTK genes, which are classified into two groups: 59 genes encode receptor PTKs (RPTKs) that possess an extracellular region, a single transmembrane segment, and a cytoplasmic region with a catalytic domain; and 32 genes encode non-receptor tyrosine kinases (NRTKs) (Fig. I.4). RPTKs serve as

receptors for growth factors and hormones. The catalytic domain of PTKs consists of two lobes in N-terminal, which interacts with the phosphate groups of ATPs, and the C-terminal domain, which provides substrate-binding sites for ATP. This domain includes the activation loop and contains Tyr residues that are to be phosphorylated. The phosphorylation of these tyrosine residues increases the kinase activity.

Classical tyrosine-specific PTPs comprise of 20 RPTPs and 18 intracellular PTPs (Alonso et al., 2004). RPTPs consist of an extracellular region, single transmembrane segment, and cytoplasmic region with one or two tyrosine phosphatase domains. RPTPs are classified into eight subfamilies (R1/R6, R2a, R2b, R3, R4, R5, R7, and R8) based on the sequence homology of their extracellular and PTP domains (Fig. I.5) (Andersen et al., 2001).

Eph receptors and ephrins in axon guidance

The Eph receptors comprise the largest subfamily of RPTKs. Eph receptors have a globular domain, a cysteine-rich domain (CRD) and two fibronectin type III repeats (FN) in the extracellular region; a kinase domain, a sterile-α-motif (SAM) and a PDZ binding motif (PBM) in the intracellular region (Flanagan and Vanderhaeghen, 1998) (Fig. I.6). Eph receptors are divided into A and B classes based on the homology of amino acid sequences and binding affinities for ephrins. In mammals, there are fourteen Eph receptors (nine EphAs and five EphBs) and eight ligands (five ephrinAs and three ephrinBs). EphrinAs are GPI-anchored proteins, characterized by the presence of a globular receptor binding domain (RBD). EphrinBs are transmembrane proteins, characterized by the presence of an extracellular RBD and intracellular PBM and five conserved tyrosine residues. Eph receptors regulate multiple developmental processes, such as tissue boundary formation, axon guidance, synaptogenesis, and blood vessel

formation (Pasquale, 2005 Arvanitis and Davy, 2008; Klein, 2012).

Abl family kinases

Abelson tyrosine kinase (Abl) family consists of two members: c-Abl and Arg (Abl-related protein) (Sefton et al.,1981; Witte et al., 1980). c-Abl kinases are composed of kinase domains, two Src homology domains in the N-terminal portion (a SH2 and a SH3 domains) and a unique N-terminal cap domain (80 amino acids) that plays an important role in the regulation of its kinase activity. c-Abl kinases also contain an actin and microtubule-binding domain, and thus c-Abl kinases have been implicated in the rearrangement of the actin and microtubule cytoskeletons *(*Van Etten et al., 1994; Wills Z et al., 1999; Woodring et al., 2003). c-Abl kinases are known to be expressed in many regions of the mammalian brain and in the growth cones of primary neurons in culture. Some reports have showed that c-Abl family kinases mediate ephrin-Eph signaling *in vivo* (Monschau et al., 1997; Connor et al., 1998). However, functional relationship between Abl family kinases and Eph receptor signaling has remained unclear.

The R3 RPTP subfamily

The R3 RPTP subfamily includes PTPRB, PTPRH, PTPRJ, and PTPRO (Fig. I.5). Previous studies including ours have revealed that R3 RPTPs are involved in the control of a variety of cellular processes, including cell growth, differentiation, axon guidance and energy metabolism (Jeon et al., 2015; Matozaki et al., 2010; Shintani et al., 2006; Shintani et al., 2015; Shintani et al., 2017). R3 RPTPs are characterized by an extracellular region composed of several fibronectin type III repeats, a transmembrane domain and a single phosphatase domain in the intracellular region (Fig. I.5). The expression of individual R3 RPTP member except for PTPRJ is restricted to a single or

limited number of tissues. PTPRB is selectively expressed in endothelial cells (EC) (Fachinger, G et al., 1999; Baumer et al., 2006). PTPRH expression is restrictedly expressed in gastrointestinal epithelial cells (Sadakata et al., 2009). PTPRO is expressed at a very high level in the kidney and brain (Van Eekelen M, et al., 2010). On the other hand, PTPRJ is widely expressed in many cell types, including endothelial, epithelial, hematopoietic, and central neuronal cells (Gaya, A, et al., 1999). Our laboratory previously revealed that all of murine R3 RPTPs recognize and dephosphorylate Eph receptors as substrate in cultured mammalian cells (Sakuraba et al., 2013).

In mice, PTPRO has been reported as a regulator of nociceptive (TrkA-positive) and proprioceptive (TrkC-positive) fibers (Gonzalez-Brito and Bixby, 2009). Mouse PTPRO also regulates survival and axonal projection of trigeminal axons through the regulation of GDNF and BDNF signaling (Gatto et al., 2013). The previous report from our laboratory has shown that chick PTPRO is implicated in the projection of retinal axons to the tectum (a homologue of the mammalian SC) through the regulation of Eph receptor activity (Shintani et al., 2006). However, *Ptpro*-deficient mice have been reported to exhibit normal retinocollicular projections (Gatto et al., 2013). Accordingly, RPTPs regulating Eph receptors in retinal axons in mammals have not yet been identified.

Purpose of my study

In this study, I investigated the roles of murine R3 RPTPs in the topographic projection of retinal axons to the brain.

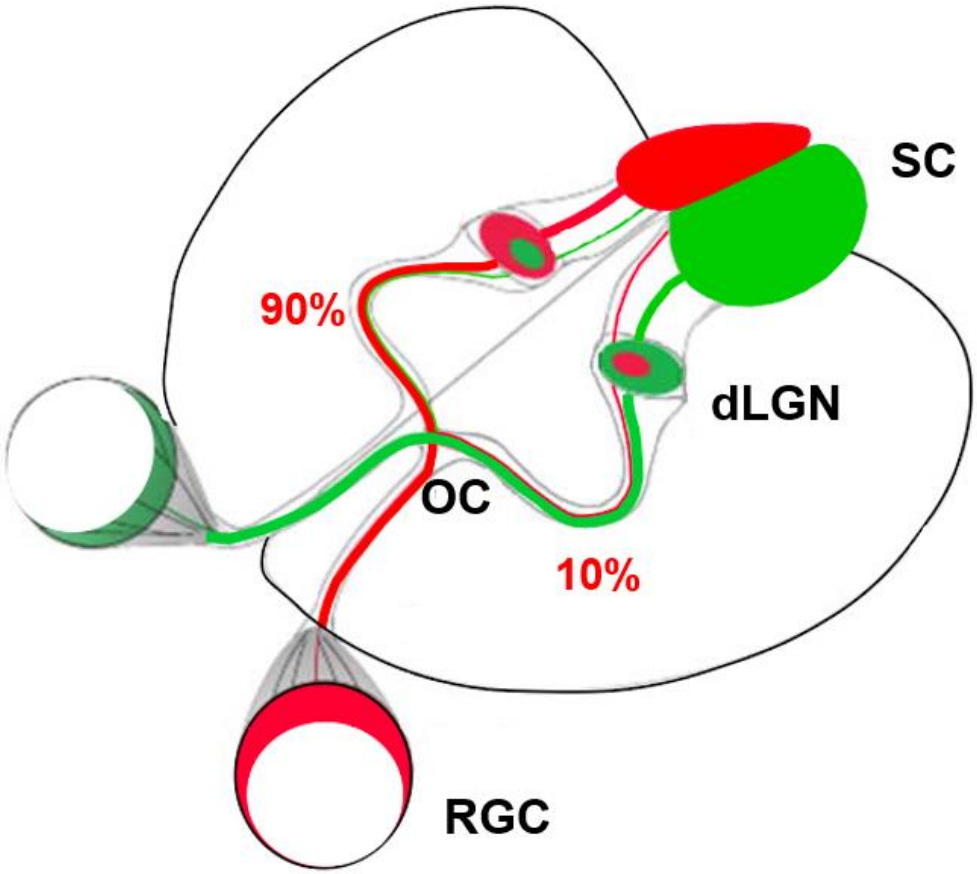

Figure I.1. General view of the visual system. Visual information is relayed from the eye to the brain via axons of retinal ganglion cells (RGCs). Retinal axons exit the eye at the optic disc and cross the midline at the optic chiasm (OC), and then extend to their targets: dorsal lateral geniculate nucleus (dLGN) in the thalamus and superior colliculus (SC) in the mid-brain in vertebrates.

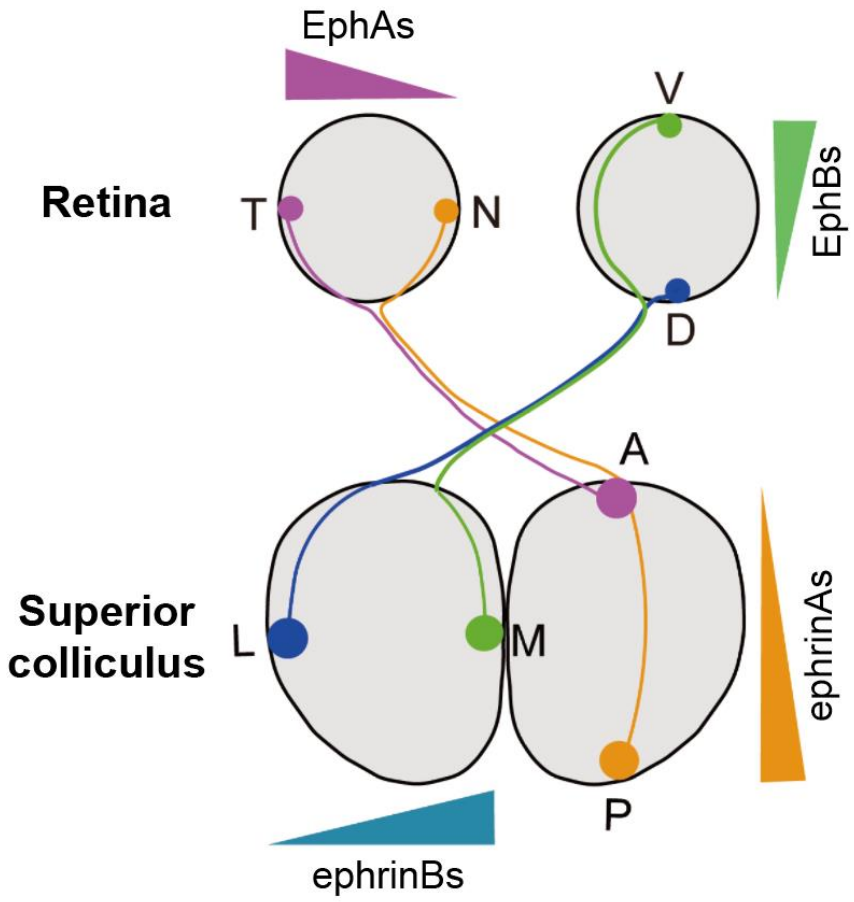

Figure I.2. A schematic drawing of the EphB1 and ephrinB2 expression in the RGCs and in the chiasm region. retinal axons from the ventrotemporal (VT) region of the retina that express EphB1 are repelled by ephrinB2 at optic chiasm (OC) and turn to the ipsilateral direction. Contralateral axons with low EphB1 expression cross the OC.

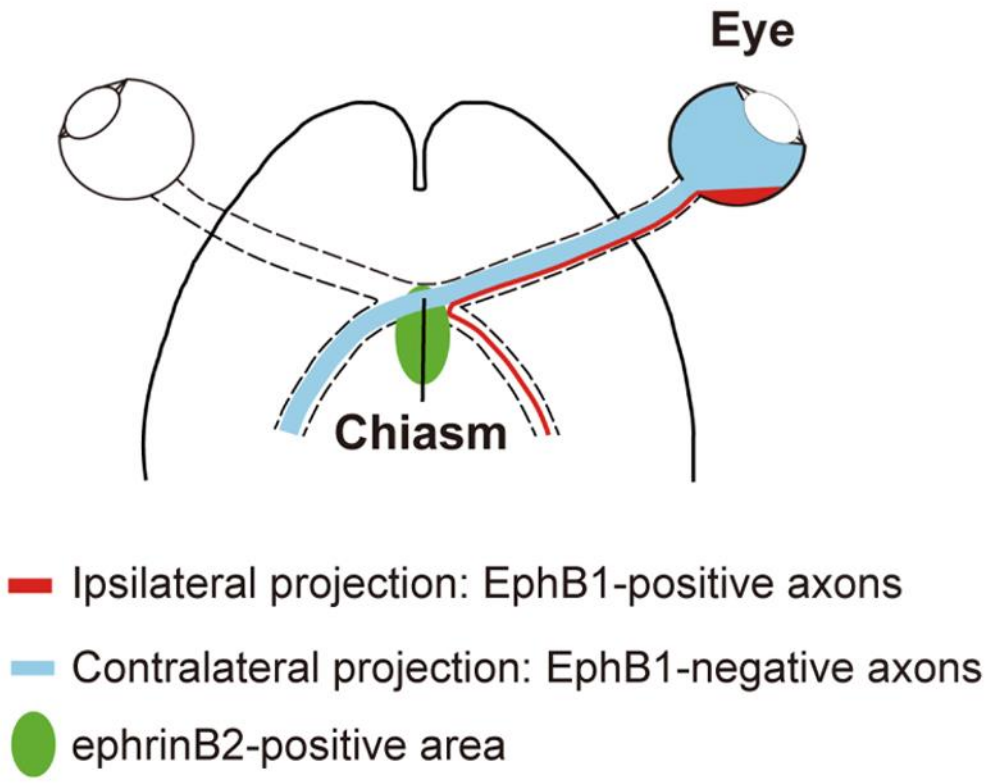

Figure I.3. Ephrin-Ephs signaling in the retinocollicular map formation. Expression patterns of Eph and ephrin in the mouse retina and superior colliculus (SC) are shown. Nasal RGC axons, expressing low levels of EphAs, project to the posterior region of the SC expressing high levels of ephrinAs, whereas temporal RGC axons with high level of EphAs terminate at the anterior part where ephrinA expression is low. Ventral RGC axons expressing low levels of EphBs terminal to the central-medial part of SC, while dorsal RGC axons with high levels of EphBs terminate at the lateral part. D, dorsal; V, ventral; N, nasal; T, temporal; SC, superior colliculus; A, anterior; P, posterior.

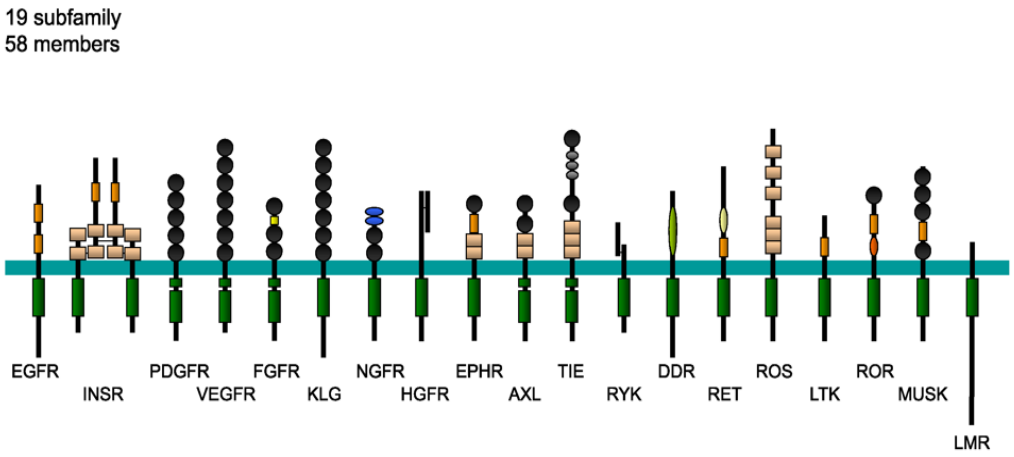

Figure I.4. Schematic diagram of the RPTK subfamilies. In humans, there exist 58 RPTKs, which are classified into 19 subfamilies based on the kinase domain sequence. All RPTKs have a similar molecular architecture, with ligand binding domains in the extracellular region, a single transmembrane helix, and a cytoplasmic region that contains the protein tyrosine kinase (PTK) domain and juxtamembrane regulatory regions.

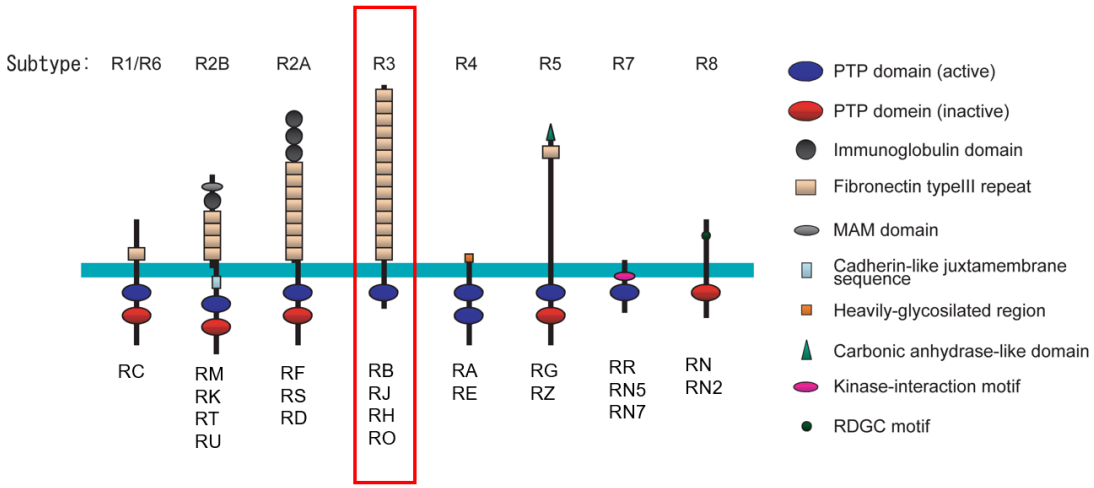

Figure I.5. Schematic diagram of the RPTP subfamilies. RPTPs consist of an extracellular domain, a single transmembrane domain, and a cytoplasmic portion with one or two tyrosine phosphatase domains. RPTPs are classified into eight subfamilies (R1-R8), based on the sequence similarity of the extracellular and PTP catalytic domains. The R3 subfamily includes PTPRB, PTPRJ, PTPRH and PTPRO. The R3 subfamily has a single PTP domain intracellularly. They share similar structures with fibronectin type III-like repeats in the extracellular region.

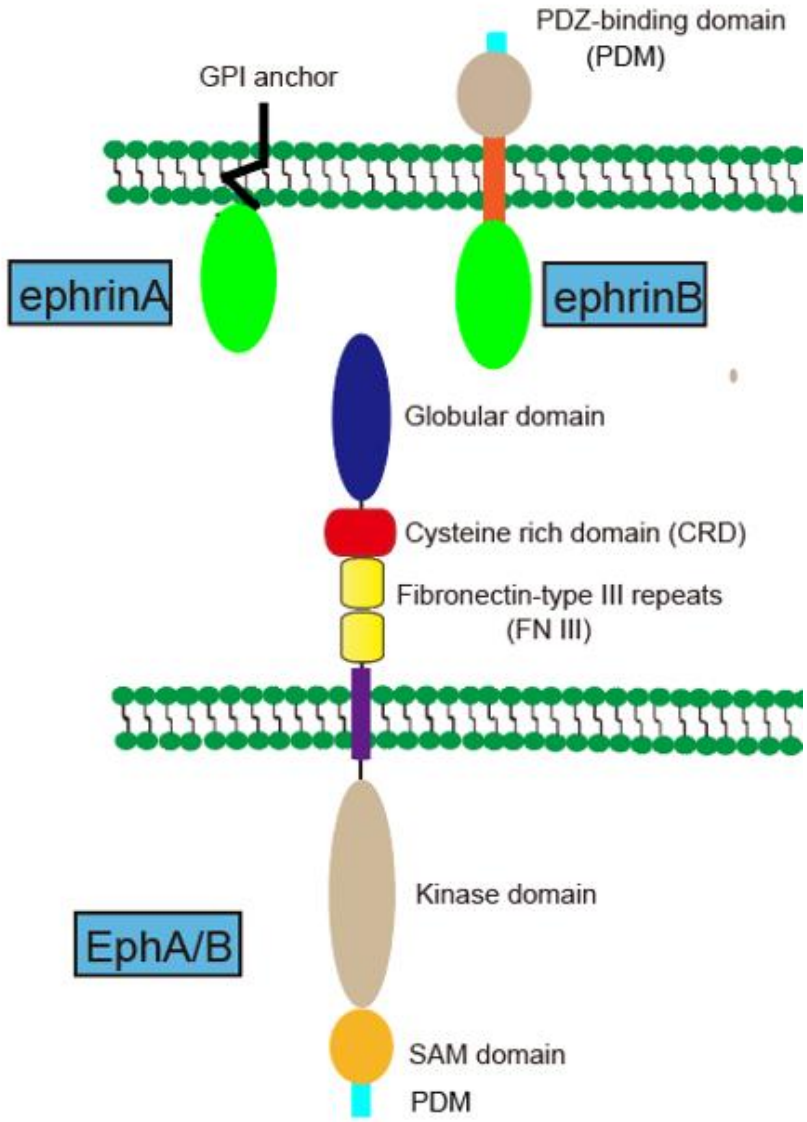

Figure I.6. A schematic drawing of the structures of Eph receptor and ephrins. The extracellular region of Eph receptors contains a globular domain, a cysteine-rich domain (CRD) and two fibronectin type III repeats (FN). The intracellular region has a tyrosine kinase domain, a SAM domain, and a PDZ binding motif (PBM). EphrinAs are GPI-anchored proteins, and ephrinBs are transmembrane proteins. Adapted from Klas Kullander, Nature reviews Molecular cell biology 2002, 3:475–486.

Materials and Methods

Mice

In the present study, *Ptprj*-KO mice generated in Dr. Fusco's laboratory (Trapasso et al., 2006) and *Ptpro*-KO mice generated in Dr. T. Shirasawa's laboratory were used in analyses. *Ptpro*-KO mice were obtained from the RIKEN Bio-Resource Center (RBRC No. 01235). These mice were backcrossed with C57BL/6J and interbred to give littermates for analyses. *Ptprj*/*Ptpro*-double-deficient mice were generated by crossing these two lines in our laboratory ($Ptprj^{+/-}Ptpro^{-/-}$ mice were interbred to obtain DKO mice). Noon on the day on which a plug was found was considered to be embryonic day (E) 0.5. All procedures were approved by the Institutional Animal Care and Use Committee of the National Institutes of Natural Sciences, Japan, and were performed in accordance with the guidelines of the Institutional Committee for the Use of Animals for Research.

Conventional and real-time (RT) quantitative PCR (RT-qPCR)

Total RNA was extracted using Trizol reagent (Life Technologies) following the manufacturer's instructions and was reverse transcribed using the PrimeScript RT reagent Kit with the gDNA Eraser (Takara). cDNAs were amplified using Ex Taq (Takara) on the T-Professional thermal cycler (Biometra, Germany) and SYBR Premix Ex Taq II (Takara) on the StepOnePlus Real-time PCR thermocycler (Applied Biosystems) for conventional and quantitative real-time PCR, respectively. Primers were designed using the Perfect Real Time support system (Takara) as follows:

Epha4, 5'-ATTGCATTCTGACAGGGTGTATGG-3' (forward) and 5'-GGCATCAATGCATAGGCACATC-3' (reverse);

Ephb2, 5'-TTTGCCTGGGTCTGAAGGTC-3' (forward) and 5'-AATTCACTAACCGATTGTTCTGCTC-3' (reverse);

Ptprb, 5'-AAACCCAGCAACTGAACCTGTTATG-3' (forward) and 5'-CAATGCAATCGTGTGGGTAGATG-3' (reverse);

Ptprh, 5'-CTGGGAACAGCAGAGCCACA-3' (forward) and 5'-CTGAGCATCCAAGGGCCAGTA-3' (reverse);

Ptprj, 5'-CCAGGTGTGGAGTGAAGCTGA-3' (forward) and 5'-GTGCACAGAACTATTGCCAGGAC-3' (reverse);

Ptpro, 5'-TGACCTTCATAAACGGTAAAGCACA-3' (forward) and 5'-ACATCCTGCCATGCCCTTG-3' (reverse);

Gapdh, 5'-ATGGCGTTTCAAAAGGCAGTGAAG-3' (forward) and 5'-TCTGCCATCACTGGTTGCAGGATC-3' (reverse). PCR settings were as follows: for conventional PCR, initial denaturation at 95°C for 30 s was followed by 28 cycles of amplification at 60°C for 30 s and at 72 °C for 30 s; for quantitative real-time PCR, initial denaturation at 95°C for 30 s was followed by 40 cycles of amplification at 95°C for 5 s and at 60 °C for 30 s. In quantitative real-time PCR, the relative quantification of gene expression was calculated relative to *Gapdh*.

In situ **hybridization**

Section *in situ* hybridization was performed as described (Shintani et al., 2012). The templates used for the preparation of cRNA probes were as follows: mouse *Ptprj*, nucleotide residues 2576-3248 (GenBank accession number NM08982) and *Ptpro*, nucleotide residues 2451-3082 (GenBank accession number XM413974).

Antibodies

The following primary antibodies were used: a mouse anti-phosphotyrosine (pTyr) antibody (polyclonal, Merck Millipore, cat# 05-321, 1:1000 dilution), rabbit anti-phosphorylated-Eph receptors (pEph) antibody (polyclonal, Abcam, cat# ab124881, 1:1000 dilution), rabbit anti-EphA2 antibody (polyclonal, Santa Cruz, cat# sc-924, 1:1000 dilution), rabbit anti-EphA3 antibody (polyclonal, Santa Cruz, cat# sc-920, 1:1000 dilution), rabbit anti-EphA4 antibody (polyclonal, Santa Cruz, cat# sc-922, 1:1000 dilution), rabbit anti-ephrinA2 antibody (Santa Cruz, cat# sc-912, 1:1000 dilution), rabbit anti-EphB1 antibody (polyclonal, Santa Cruz, cat# sc-926, 1:1000 dilution), rabbit anti-EphB2 antibody (polyclonal, Santa Cruz, cat# sc-28980, 1:1000 dilution), rabbit anti-ephrinB2 antibody (polyclonal, Santa Cruz, cat# sc-1010, 1:1000 dilution), mouse anti-acetylated α-Tubulin antibody (monoclonal, Santa Cruz, cat# sc-23950, 1:1000 dilution), mouse anti-β-Tubulin III antibody (monoclonal, Sigma-Aldrich, cat# T8660, 1:1000 dilution), rabbit anti-c-Abl antibody (polyclonal, Cell Signaling Technology, cat# 2862S, 1:1000 dilution), and rabbit anti-phosphorylated c-Abl (pAbl) antibody (monoclonal, Cell Signaling Technology, cat# 2865S, 1:1000 dilution). Peroxidase-conjugated secondary antibodies were from GE Healthcare.

Immunoprecipitation, pull-down, and Western blotting

Immunoprecipitation experiments were performed as described (Shintani et al., 2006). In brief, the retinas of postnatal day (P) 8 mice were lysed in lysis buffer, which consisted of 20 mM Hepes, pH 7.4, 120 mM NaCl, 1% Nonidet P-40, 50 mM NaF, 0.5 mM Na_3VO_4, and a protease inhibitor mixture (10 μg/ml leupeptin, 1 μg/ml pepstatin A, and 1 mM phenylmethylfonyl sulfate). Protein concentrations were measured with a BCA microassay kit (Life Technologies). Regarding immunoprecipitation, retinal lysates were incubated with anti-pTyr antibody and immunoprecipitates were collected

with Protein G magnetic beads (Thermo Fischer Scientific). Pull-down experiments were performed as described (Himanen et al., 2004). In brief, 10 μg of the ephrinA2-Fc or ephrinB2-Fc proteins was incubated with retinal lysates containing 2 mM $MgCl_2$, and pull-down complexes were collected with Protein G magnetic beads. Proteins were subjected to SDS-polyacrylamide gel electrophoresis and Western blotting (Shintani et al., 2006). Separated proteins were transferred onto Immobilon-P membranes (Merck Millipore), incubated with specific primary antibodies and peroxidase-conjugated secondary antibodies (GE Healthcare), followed by detection with chemiluminiscence using ECL Reagent (Perkin Elemer). The lumino-image analyzer LAS-5000 (Fujifilm) was used for detection. Signal intensity was quantified by densitometry.

DNA constructs

Myc-tagged mouse *c-Abl* cDNA was cloned by RT-PCR and subcloned into the expression vector pcDNA 3.1 (Thermo Fischer Scientific). RPTP constructs were described previously (Sakuraba et al., 2013).

Cell cultures and transfection

HEK293T cells were grown in DMEM/F-12 medium supplemented with 10% fetal bovine serum (FBS) and antibiotics. Transfection was performed using LipofectAMINE PLUS (Invitrogen) according to the protocol of the manufacturer. After being cultured for 24 h, cells were subjected to Western blotting as described above.

DiI labeling

Optic tract DiI (1,1'-dioctadecyl-3,3,3',3'-tetramethyl-indocarbocyanine perchlorate,

Thermo Fischer Scientific) labeling experiments were performed as previously described (Anderson et al., 1998; Plump et al., 2002). In brief, the heads were removed at E17.5 or P1, and fixed in 10% formaldehyde at room temperature overnight. The lens and retinas of the left eye were then removed, and small crystals of DiI labeling were placed directly on the optic disc. The tissue was incubated in 10% formaldehyde at room temperature and kept in the dark for 10 days. After the incubation, the ventral diencephalon containing the optic nerve was dissected out, and images were acquired with an LSM 700 laser scanning confocal microscope (Carl Zeiss). The index of projections to the ipsilateral side was calculated by dividing the fluorescent intensity of the ipsilateral optic tract by the total fluorescent intensity of both tracts (Soskis et al., 2012; see Fig. II.5A, middle). The index of projections to the contralateral retina was calculated by dividing the fluorescent intensity of the left optic nerve by the fluorescent intensity of the right optic nerve (see Fig. II.5A, right).

In the analysis of retinocollicular projections, anterograde focal retinal DiI labeling was performed as previously described (Brown et al., 2000). Briefly, mice at P8 were anesthetized on ice, and a small amount of 10% DiI in dimethylformamide was injected into the peripheral region of the retina. After 48 h, the whole brain containing the SC and retina was dissected out, and then fixed in 10% formaldehyde at 4°C for 16 h. Images were acquired with an LSM 700 laser scanning confocal microscope. The center of fluorescence (center of mass) for each image was calculated and used to define the position of the terminal zone (TZ) in the SC along the A-P axis, which ranged between 0 and 20 (see Fig. II.6U, Fig. II.7U and Fig. II.8U).

Growth cone collapse assay

A retinal strip culture was performed as previously described (Shintani et al., 2006).

Briefly, retinal strips (width, 400 μm) prepared from E16.5-E17.5 retinas were cultured in DMEM containing 10% FBS on laminin (20 μg/ml)-coated dishes in a humidified incubator with 5% CO_2 for 2 d. Axons and growth cones were stimulated with ephrinA2-Fc or control Fc (0-10 μg/ml, final concentration) at 37°C for 30 min. A pretreatment with DPH (20 μg/ml, Sigma-Aldrich) or imatinib (10 μg/ml, Sigma-Aldrich) was performed for 15 min prior to the stimulation with ephrinA2-Fc. After fixation with 4% parformaldehyde in PBS for 10 min, the strips were stained with an anti-β-III tubulin antibody and Alexa594-phalloidin (Thermo Fischer Scientific). Images were observed with a Zeiss LSM700 confocal laser microscope.

Retinal explant cultures

Retinal explant cultures were performed as described (Wang et al., 1995). In brief, the ventrotemporal region of the retina was dissected from E15.5 embryos and cultured in collagen I gels (Nitta gelatin) containing 2 μg/ml of ephrinB2-Fc or control Fc proteins for 48 h. After fixation with 4% parformaldehyde in PBS for 10 min, neurites were staining with an anti-βIII tubulin antibody. Images were observed with a Zeiss LSM700 confocal laser microscope. The total area covered by neurites was quantified with ImageJ software.

For quantification of neurite outgrowth in explant cultures, the total area covered by neurites of individual explants was quantified by measuring pixel intensity with ImageJ software. Each experiment was carried out three times, and within each experiment, at least six explants were treated in each experimental group.

Primary culture of retinal neurons.

Retinas dissected from E16.5-E17.5 mice were digested with 0.1% trypsin in PBS at

37°C for 15 min. After adding 10 volumes of DMEM containing 10% FBS, neurons were mechanically dissociated into single cells by pipetting. The dissociated neurons were plated on laminin (20 μg/ml)-coated dishes at a density of 1×10^6 cells/ml and maintained in Neurobasal medium (Thermo Fischer Scientific) supplemented with B27 supplement (Thermo Fischer Scientific) for 48 h. Retinal neurons were stimulated with ephrinA2-Fc or control Fc (10 μg/ml, final concentration) at 37°C for 30 min, and proteins were then extracted and subjected to Western blotting as described above.

***In vitro* dephosphorylation assay.**

GST-fusion proteins encoding the entire intracellular region of RPTPs were described previously (Sakuraba et al., 2013). Regarding *in vitro* dephosphorylation, I prepared autophosphorylated c-Abl proteins as the substrate. Phosphorylated c-Abl proteins were purified from HEK293T cells expressing Myc-tagged c-Abl by immunoprecipitation with an anti-Myc antibody and protein G-Sepharose CL-4B. Protein G beads were washed three times with lysis buffer and re-suspended in 100 μl of 10 mM Tris–HCl, pH 7.0, containing 5 mM DTT, 5 mM EDTA, and 100 μg/ml bovine serum albumin (PTP buffer). In the dephosphorylation assay, 10 ng of GST-RPTPs or GST alone was reacted with 10 μl of the phosphorylated c-Abl protein solution at 30°C for 15 min. The reaction was stopped by adding SDS sample buffer. The samples were separated by SDS–PAGE followed by Western blotting with anti-phosphotyrosine and anti-Myc antibodies.

Experimental Design and Statistical Analysis.

The sample size was calculated from a power analysis using preliminary data obtained in our laboratory under the following assumptions: $\alpha = 0.05$ and power = 0.8. Statistical

analyses were performed using the Student's *t*-test or ANOVA followed by Tukey's post hoc test using Prism 5 (GraphPad Software). All the Results are presented as the mean ± SEM. $P < 0.05$ was considered to be significant.

Results

Expression of R3 RPTPs in the developing retina

I examined the expression levels of R3 subfamily members of RPTPs in the developing retina. RT-PCR analyses of the retina on postnatal day 0 (P0) revealed the gene expression of *Ptprj* and *Ptpro*, but not of *Ptprb* or *Ptprh* (Fig. II.1C). These results were consistent with previous findings showing that PTPRJ and PTPRO are expressed in the central nervous system (Beltran et al., 2003; Gaya et al., 1999) and that the expression of PTPRB and PTPRH is restricted to endothelial and intestinal epithelial cells, respectively (Fachinger et al., 1999; Sadakata et al., 2009).

Ptprj and *Ptpro* mRNAs were detected in the ganglion cell layer (GCL) and inner nuclear layer (INL) (Fig. II.1D): There appeared to be no expression gradient along the antero-posterior or dorso-ventral axis. Color development for *Ptpro* mRNA required more time (~24 h) than that for *Ptprj* (~5 h), which reflected the lower expression level of *Ptpro* than that of *Ptprj*.

The gene expression of *Ptprj*, *Ptpro*, and Eph receptors during retinal development was examined using RT-qPCR. *Ptprj* mRNA peaked on P0 in the retina, and gradually decreased thereafter (Fig. II.1E, left). *Epha4* and *Ephb2* mRNAs showed a similar expression level and pattern to *Ptprj* mRNA (Fig. II.1E, right); expression peaked on P0 and gradually decreased thereafter. However, the expression level of *Ptpro* mRNA was markedly lower than those of other mRNAs, and its expression pattern differed (Fig. II.1E, middle); *Ptpro* expression gradually increased and peaked on P4.

Up-regulation of tyrosine phosphorylation of Eph receptors in retinas of *Ptprj*-KO

and *Ptprj*/*Ptpro*-KO mice

In order to establish whether PTPRO and/or PTPRJ are involved in the regulation of Eph signaling in the retina, I investigated abnormalities in *Ptpro*-KO, *Ptprj*-KO, and DKO mice. The retinal layer structures of these knockout mice were normal (Fig. II.2A), and these mice had the same eyeball size at birth (data not shown). These results suggested that a deficiency in *Ptpro* or *Ptprj* did not have any effects on the development of the retinal architecture. WT and three knockout mice showed similar expression levels of EphA4, EphB2, ephrinA2, and ephrinB2 proteins in the P8 retina (Fig. II.2B).

I examined the phosphotyrosine levels of proteins in the retina by Western blotting. No significant differences were detected in total phosphotyrosine levels (Fig. II.2C, left). In order to compare the phosphotyrosine levels of Eph receptors, tyrosyl-phosphorylated proteins were immunoprecipitaed with an anti-phosphotyrosine antibody, and then analyzed using an antibody to anti-tyrosyl-phosphorylated EphA/B receptors. Phosphorylated Eph receptors were most prominently detected at ~120 kDa in each immunoprecipitated sample (Fig. II.2C, center). Our laboratory previously reported that mouse PTPRO and PTPRJ dephosphorylated Eph receptors in cultured cells (Sakuraba et al., 2013). The *Ptpro*-KO retina showed a similar phosphotyrosine level of Eph receptors with the WT retina (120 % of WT, $p = 0.59$) (120 % of WT, $p = 0.59$) (Fig. II.2C, right). On the other hand, the phosphotyrosine level of Eph receptors in the *Ptprj*-KO retina and DKO were significantly higher than that in the WT retina (*Ptprj*-KO, 158%, $p = 0.014$; DKO, 200%, $p = 0.0002$).

I next examined the phosphotyrosine levels of EphAs and EphBs separately. To this end, I performed pull-down experiments with ephrin-Fc proteins. EphB and EphA receptors were purified with ephrinB2-Fc and ephrinA2-Fc proteins, respectively, and

then analyzed using the antibodies to anti-tyrosyl-phosphorylated EphA/B receptors. The *Ptpro*-KO retina showed a similar phosphotyrosine level of EphB receptors with the WT retina (113 ± 12% of WT, p = 0.93) (Fig. II.2D). On the other hand, the phosphotyrosine levels of EphB receptors in the *Ptprj*-KO and DKO retina were significantly higher than those in the WT retina (*Ptpro*-KO, 113 ± 12%, p = 0.93; *Ptprj*-KO, 191 ± 10%, p = 0.006; DKO, 208 ± 27%, p = 0.002) (Fig. II.2D). In addition, the *Ptpro*-KO retina showed a similar phosphotyrosine level of EphB receptors with the WT retina (114 % ± 7% of WT, p = 0.74), while the phosphotyrosine levels of EphA receptors were significantly higher in the *Ptprj*-KO and DKO retina than those in the WT retina (*Ptprj*-KO, 182 ± 13%, p = 0.0002; DKO, 194 ± 12%, p = 0.0001) (Fig. II.2E).

PTPRJ suppresses the sensitivity of VT retinal axons to ephrinB2

Retinal axons from the VT retinal region express high levels of the EphB receptor to sense ephrinB2 at the chiasm, and thereby turn ipsilaterally (Fig. II.1A). To clarify whether the deficiency of PTPRO or PTPRJ affects the sensitivity of VT retinal axons to ephrinB2, I examined neurite outgrowth from VT retinal explants prepared from WT, *Ptpro*-KO, *Ptprj*-KO, and DKO mice (Fig. II.3). In control Fc, many long neurites extended from the VT explants, and no significant differences were observed in the neurite outgrowth among the four genotypes (Fig. II.3A, B). Moreover, I also observed a marked reduction in neurite outgrowth from all VT explants when cultured on ephrinB2-Fc (Fig. II.3A, C). Neurite outgrowth from the explants was strongly suppressed in *Ptprj*-KO and DKO mice than in WT or *Ptpro*-KO mice (WT, 2.3 ± 0.3; *Ptpro*-KO, 2.1 ± 0.3, p = 0.95; *Ptprj*-KO, 0.5 ± 0.1, p = 0.0002; DKO: 0.4 ± 0.1, p = 0.0001) (Fig. II.3C), which is consistent with the results obtained for the tyrosine

phosphorylation levels of EphB receptors in *Ptpro*-KO and DKO mice (Fig. II.2D). These results indicated that activities of EphB1 receptors in VT RGC axons are mainly regulated by PTPRJ.

PTPRJ suppresses the sensitivity of retinal axons to ephrinA2 and ephrinA5

I examined growth cone collapse induced by ephrinA2-Fc or ephrinA5-Fc using axons growing from the cultured stripes of retinas prepared from WT, *Ptpro*-KO, *Ptprj*-KO, and DKO mice (Fig. II.4). Figure II.4A and B show representative responses of WT retinal axons to ephrinA2 and ephrinA5, respectively. Control Fc protein gave no effect on the collapse rate of nasal and temporal axons (Fig. 4.II.C, D; left). Stimulation with ephrinA2-Fc (2.50 g/ml) markedly increased the collapse rate of nasal and temporal axons of all genotypes (Fig 4.II.C, D; center). Nasal and temporal axons of *Ptpro*-KO mice did not show significant differences in the collapse rate with those of WT mice (nasal axons: WT, 38 ± 2%; *Ptpro*-KO, 44 ± 5%, $p = 0.48$ / temporal axons: WT, 57 ± 2%; *Ptpro*-KO, 52 ± 5%, $p = 0.70$) (Fig. 4.II. C, D). However, nasal and temporal axons of *Ptprj*-KO and DKO mice both exhibited significantly higher collapse rates than those of WT (nasal axons: *Ptprj*-KO, 52 ± 2%, $p = 0.008$; DKO, 60 ± 5%, $p = 0.0003$ / temporal axons: *Ptprj*-KO, 68 ± 2%, $p = 0.047$; DKO, 80 ± 3%, $p = 0.00004$) (Fig. Fig. 4.II. C, D).

There was also no significant difference in the collapse rate of nasal and temporal axons with ephrinA5-Fc (1.25 μg/ml) between *Ptpro*-KO and WT mice (nasal axons: WT, 34 ± 3%; *Ptpro*-KO, 27 ± 3%, $p = 0.75$ / temporal axons: WT, 52 ± 2%; *Ptpro-KO*, 53 ± 2%, $p = 0.99$) (Fig. 4.II C, D). In contrast, nasal and temporal axons of *Ptprj*-KO and DKO mice exhibited significantly higher collapse rates than those of WT mice (nasal axons: *Ptprj*-KO, 48 ± 2%, $p = 0.010$; DKO, 46 ± 2%, $p = 0.032$ / temporal axons:

Ptprj-KO, 65 ± 1%, $p = 0.003$; DKO, 67 ± 3%, $p = 0.0007$) (Fig. 4.II C, D). Based on the dose dependency experiments (data not shown), ephrinA5 appeared to be more active to retinal axons than ephrinA2.

Collectively, these results indicated that PTPRJ mainly influences the sensitivity of both nasal and temporal retinal axons to ephrinAs by controlling the activity of EphA receptors, which is consistent with the tyrosine phosphorylation levels of Eph receptors in *Ptpro*-KO and DKO mice (Fig. II.2E). Expectedly, temporal axons showed higher sensitivity to ephrinAs than nasal axons in all groups.

PTPRJ is involved in the crossing decision of retinal axons at the OC

The OC is an important midline decision point for sorting retinal axons that project whether ipsilaterally or contralaterally. EphB signaling has been implicated in axonal selection in the root at the OC (Williams et al., 2003). I performed the anterograde DiI labeling of RGC axons from the right eye at E17.5 and P1 because most retinal axons have passed through the OC at E17.5, and contralateral and ipsilateral tracts are both established at P1 (Godement et al., 1987) (Fig. II 5A). Whole-mount views of the OC revealed marked differences in the sorting of axons between DKO and WT mice: The proportion of axons projecting ipsilaterally markedly increased in DKO mice (arrows, Fig.II 5B, C). I measured the relative fluorescence of the ipsilateral optic tract and the total fluorescence intensities of both optic tracts as the ipsilateral index (see the right panel in Fig. II.5A). At E17.5, no significant differences in the ipsilateral index were observed between *Ptpro*-KO, *Ptprj*-KO, and WT mice (WT, 8.8 ± 1.7%; *Ptpro*-KO, 8.6 ± 1.7%, $p = 1.0$; *Ptprj*-KO, 13.7 ± 3.1%, $p = 0.64$) (Fig. II.5D). However, the ipsilateral index of DKO mice was significantly higher than that of WT mice (WT, 8.8 ± 1.7%; DKO, 24.5 ± 4.3%, $p = 0.015$) (Fig. II.5D).

When labeled at P1, the proportion of axons projecting ipsilaterally were significantly increased in *Ptprj*-KO and DKO mice (WT, 7.8 ± 0.6%; *Ptpro*-KO, 8.7 ± 1.2%, $p = 0.97$; *Ptprj*-KO, 13.3 ± 1.7%, $p = 0.032$; DKO, 13.6 ± 1.5%, $p = 0.013$) (Fig. II.5E). However, no significant differences were observed in ipsilateral projections between *Ptpro*-KO and WT mice (Fig. II.5E). These results suggested that PTPRJ functions to confine ipsilateral projections by controlling EphB activity.

PTPRJ is involved in the prevention of axon misrouting to the opposite eye

In addition to increased ipsilateral projections, I found that larger proportions of RGC axons projected to the contralateral eye in *Ptprj*-KO and DKO mice than in WT mice (asterisks, Fig. II.5B, C). Therefore, I measured relative fluorescence in the contralateral (left) optic nerves vs. the right optic nerve as the misrouting index (see the right panel in Fig. II.5A). At E17.5, *Ptprj*-KO and DKO mice, but not *Ptpro*-KO mice showed a significantly higher index than WT mice (WT, 6.3 ± 1.0%; *Ptpro*-KO, 13. 7 ± 4.2%, $p = 0.78$; *Ptprj*-KO, 32.6 ± 7.0%, $p = 0.009$; DKO, 40.4 ± 7.5%, $p = 0.0005$) (Fig. II.5F). On P1, the proportion of axons projecting the contralateral optic nerve remained significantly higher in *Ptprj*-KO and DKO mice (WT, 6.5 ± 0.7%; *Ptpro*-KO, 8.9 ± 1.3%, $p = 0.068$; *Ptprj*-KO, 13.1 ± 1.8%, $p = 0.018$; DKO, 16.9 ± 2.0%, $p = 0.0001$) (Fig. II.5G). However, the retinal axons of *Ptpro*-KO mice again showed no significant difference by itself in projections to the contralateral optic nerve (Fig. II.5G). These results suggested that PTPRJ suppresses axon misrouting to the contralateral optic nerve.

PTPRJ regulates the topographic mapping of retinal axons in the SC

In order to elucidate whether PTPRO and/or PTPRJ are involved in topographic

retinocollicular projections in the SC, retinocollicular projections on P10 were investigated by anterograde labeling with DiI. Small focal injections of DiI were performed into the retina on P8, when retinocollicular projections have matured in mice (Hindges et al., 2002; Simon and O'Leary, 1992), and the contralateral SC was examined 48 h later (Fig. II.6).

In WT mice, a single retinal injection of DiI into the nasal periphery of the retina exhibited a single DiI-labeled TZ in the posterior area of the contralateral SC in all mice (11 of 11) (Fig. II.6A-C). A sagittal section of the SC showed that nasal axons formed terminal arbors in the superficial layer in the posterior SC (Fig. II.6D, E). In all *Ptpro*-KO mice (11 out of 11), nasal axons developed proper TZs in the posterior SC, similar to WT mice (Fig. II.6F-J). However, large proportions of nasal axons formed TZs at more anterior locations within the SC in *Ptprj*-KO and DKO mice (Fig. II.6K-M, P-R). Sagittal sections clearly showed that axons from the nasal retina formed anteriorly shifted major TZs, in addition to minor TZs at the appropriate topographic location in the posterior part of the SC in *Ptprj*-KO (4 out of 11) and DKO mice (6 out of 11) (Fig. II.6N, O, S, T). A quantitative analysis of the distribution of TZs on the SC revealed that *Ptprj*-KO and DKO mice, but not *Ptpro*-KO mice, exhibited TZs that had anteriorly shifted more prominently than those of WT mice (WT, 0.9 ± 0.1; *Ptpro*-KO, 0.9 ± 0.1, $p = 0.99$; *Ptprj*-KO, 1.5 ± 0.2, $p = 0.026$; DKO, 2.0 ± 0.2, $p = 0.0001$) (Fig. II.6U).

I then examined projections from the ventral retinal regions: RGC axons from the ventral retina normally project to the medial part of the contralateral SC. Ventral retinal injections of DiI in WT mice revealed a single TZ located midway along the A-P axis within the medial SC (11 out of 11) (Fig. II.7A-C). A sagittal section of the SC indicated that labeled WT axons formed terminal arbors in the superficial layer in the medial SC (Fig. II.7D, E). In *Ptpro*-KO mice (11 out of 11), ventral axons developed TZs in the

medial SC, similar to WT mice (Fig. II.7F-J).

In contrast, in large proportions of *Ptprj*-KO and DKO mice, ventral retinal axons showed anteriorly shifted TZs within the SC (Fig. II.7K-M, P-R). Sagittal sections showed that ventral retinal axons also formed anteriorly shifted TZs in addition to normal TZs in the medial part of the SC in *Ptprj*-KO (4 out of 11) and DKO mice (7 out of 11) (Fig. II.7N, O, S, T). A quantitative analysis of the distribution of TZs on the SC revealed that the TZs of *Ptprj*-KO and DKO mice, but not *Ptpro*-KO mice, had significantly shifted anteriorly (WT, 9.0 ± 0.46; *Ptpro*-KO, 9.2 ± 0.4, $p = 0.98$; *Ptprj*-KO, 11.3 ± 0.5, $p = 0.005$; DKO, 12.8 ± 0.5, $p = 0.0001$) (Fig. II.7U).

Regarding temporal retinal axons, the temporo-peripheral retinal axons project to the most anterior region of the SC and difficulties are associated with detecting alterations in their projection. Therefore, I examined projections from the centrotemporal retinal regions (Fig. II.8). In WT mice, the centrotemporal retinal injections of DiI gave rise to a single TZ located in the anterior area (11 out of 11) (Fig. II.8A-C). Sagittal section of the SC indicated that labeled WT axons formed terminal arbors in the superficial layer in the SC (Fig. II.8D, E). In *Ptpro*-KO mice (11 out of 11), I observed single TZs in the anterior SC, similar to WT mice (Fig. II.8F-J). In contrast, in large proportions of *Ptprj*-KO and DKO mice, centro-temporal retinal axons showed anteriorly shifted TZs within the SC (Fig. II.8K-M, P-R). Sagittal sections also exhibited that centro-temporal retinal axons formed anteriorly shifted TZs in addition to normal TZs in the anterior part of the SC in *Ptprj*-KO (5 out of 11) and DKO mice (6 out of 11) (Fig. II.8N, O, S, T). A quantitative analysis of the distribution of TZs on the SC revealed that the TZs of *Ptprj*-KO and DKO mice, but not *Ptpro*-KO mice, had significantly shifted anteriorly (WT, 16.7 ± 0.3; *Ptpro*-KO, 16.9 ± 0.2, $p = 0.97$; *Ptprj*-KO, 17.8 ± 0.2, $p = 0.015$; DKO, 17.9 ± 0.1, $p = 0.0007$) (Fig. II.8U).

Thus, altered anteroposterior mapping, was evident in the retinocollicular projections of *Ptprj*-KO and DKO mice, suggesting that the retinal axons of *Ptprj*-KO and DKO mice had hypersensitivity to ephrinAs distributed gradiently along the A-P axis in the SC. However, no obvious alterations were detected along the M-L axis in all retinal axons tested in all genotypes.

c-Abl activity is involved in ephrin-induced growth cone collapse of retinal axons and PTPRJ controls c-Abl activity

c-Abl kinases consisting of c-Abl (Abelson) and Arg (Abl related gene) are a unique family of non-receptor-type tyrosine kinases. Their C-terminal portion harbors an actin-binding domain, and, thus, c-Abl kinases have been implicated in the rearrangement of the actin cytoskeleton *(*Wills et al., 1999; Woodring et al., 2003). In cancer cells and intestinal stem cells, ephrin-Eph signaling is reportedly mediated by c-Abl (Noren et al., 2006; Genander et al., 2009). In retinal axons, ephrinA5-induced growth cone collapse is inhibited by the c-Abl inhibitor, STI571 (imatinib) (Harbott and Nobes, 2005). However, the role of c-Abl in Eph signaling in retinal axons has remained unclear.

In order to reveal the functional significance of c-Abl in Eph signaling in retinal axons, I examined the activation of c-Abl after the stimulation of Eph receptors with ephrinB2 or ephrinA2 using dissociated retinal neurons. The phosphorylation at tyrosine 412 (Y412) in the activation loop of c-Abl was assessed as an indicator of the activation of c-Abl. An anti-tyrosyl-phosphorylated-c-Abl antibody (anti-pAbl) detected a band of approximately 135 kDa, the predicted size of c-Abl (Fig. II.9A). The treatment with ephrinB2-Fc increased the phosphorylation level of c-Abl in retinal cells 1.2 ± 0.1 fold ($p = 0.23$) at 15 min and 1.7 ± 0.2 fold ($p = 0.001$) at 30 min (Fig. II.9A).

The stimulation of dissociated retinal cells with ephrinA2-Fc proteins also induced the activation (phosphorylation) of c-Abl within 15 min (1.6 ± 0.2 fold, $p = 0.022$), and the phosphorylation level was sustained for at least 30 min (1.8 ± 0.1 fold, $p = 0.004$) (Fig. II. 9B). These results suggested that c-Abl was activated by ephrin-Eph signaling.

In order to test whether PTPRO and PTPRJ directly dephosphorylate c-Abl as well as Eph receptors, I performed *in vitro* experiments using purified proteins. GST-PTPRO and GST-PTPRJ both efficiently dephosphorylated c-Abl proteins prepared from HEK293T cells by immunoprecipitation (GST, 1; GST-PTPRO, 0.40 ± 0.05, $p = 0.001$; GST-PTPRJ, 0.43 ± 0.07, $p = 0.001$) (Fig. II.9C). These results indicated that PTPRO and PTPRJ dephosphorylated specific phosphotyrosine residues in c-Abl proteins. Furthermore, I performed coimmunoprecipitation experiments using wild-type (WT) and substrate-trapping DA mutants of PTPRO and PTPRJ: the DA mutant in which the general aspartic acid (D) residue in the PTP domain is converted to alanine (A) is deficient in the PTPase activity but retains the ability to recognize and stably bind substrates (Flint et al., 1997). The DA mutants of PTPRO and PTPRJ, but not the WT, coimmunoprecipiated with c-Abl (Fig. II.9D), indicating that c-Abl is recognized as a substrate by PTPRO and PTPRJ in cells. Furthermore, when c-Abl was co-expressed together with full-length PTPRO or PTPRJ in HEK293T cells, the tyrosine phosphorylation levels of c-Abl were significantly reduced (WT, 1; PTPRO, 0.46 ± 0.08, $p = 0.002$; PTPRJ, 0.27 ± 0.05, $p = 0.0001$) (Fig. II.9E). Together, these results indicated that PTPRO and PTPRJ dephosphorylate c-Abl as a physiological substrate.

I confirmed the phosphotyrosine levels of c-Abl in the retinas between the knockout mice. Western blotting verified that the expression levels of c-Abl were similar in P8 retinas of WT and knockout mice (Fig. II.9F). Expectedly, pAbl levels in *Ptprj*-KO and DKO retinas were significantly higher than those in WT retinas (WT, 1;

Ptpro- KO, 1.29 ± 0.12, $p = 0.497$; *Ptprj*- KO, 1.69 ± 0.17, $p = 0.028$; DKO, 2,07 ± 0.21, $p = 0.001$) (Fig. II.9F). These results indicated that PTPRJ predominantly regulates c-Abl activity in the retina, and that the abnormal projections of retinal axons observed in *Ptprj*-KO and DKO mice were attributable to the aberrant activation of c-Abl in these mice.

I then investigated whether c-Abl is necessary for the transduction of repellant signal by Eph receptors in retinal axons. I first examined whether the inhibition of neurite outgrowth from the VT retinal explants by ephrinB2 was ameliorated by a treatment with imatinib (c-Abl inhibitor) or DPH (c-Abl activator) (Yang et al., 2011; Dun et al., 2015; Liu et al., 2017) using VT retinal explants. The imatinib treatment had no effect on the neurite extension on the control Fc, but significantly suppressed the inhibition of neurite outgrowth by ephrinB2-Fc (0.7 ± 0.2 vs. 4.0 ± 0.3, $p = 0.000001$) (Fig. II.10A). The treatment with DPH markedly inhibited neurite extension from the VT explants (7.2 ± 0.5 vs. 1.3 ± 0.1, $p = 0.000003$), and DPH slightly enhanced the effects of ephrinB2-Fc on neurite extension (1.0 ± 0.2 and 0.2 ± 0.1, $p = 0.047$) (Fig. II.10A). These results implicated c-Abl kinase in the inhibition of neurite extension by ephrinB2.

I next investigated whether ephrinA2-induced growth cone collapse was affected by a treatment with imatinib or DPH using temporal retinal axons. The imatinib treatment had no effect on the basal growth cone collapse rate, but significantly suppressed that induced by ephrinA2-Fc (31 ± 3% and 21 ± 1%, $p = 0.0001$) (Fig. II.10B). The treatment with DPH alone increased the collapse rate (9 ± 1% to 39 ± 2%, $p = 0.001$), and DPH enhanced the effects of ephrinA2-Fc on growth cone collapse (39 ± 2% and 70 ± 1%, $p = 0.001$) (Fig. II.10B). These results suggested that c-Abl kinase

plays a pivotal role in the growth cone collapse of retinal axons induced by ephrinA molecules.

Activation of c-Abl induces abnormal axonal projections similarly to those observed in *Ptprj*-KO and DKO mice

I finally investigated whether the forced activation of c-Abl kinases *in vivo* induces similar abnormal retinal projections to those observed in *Ptprj*-KO and DKO mice. I injected DPH (20 mg/kg) into pregnant mice daily between E11.5 and E16.5, and embryos were fixed and analyzed at E17.5. In DPH-treated embryos, the proportion of axons projecting ipsilaterally markedly increased (ipsilateral index: control, 14.0 ± 1.2%; DPH-treated: 23.7 ± 2.4%, p = 0.004) (Fig. II.11A, B). Furthermore, the proportion of axons projecting into the contralateral optic nerve also significantly increased in DPH-treated mice (misrouting index: control, 4.6 ± 0.9 %; DPH-treated, 8.9 ± 1.4%, p = 0.028) (Fig. II.11A, C). These phenotypes were similar to those in *Ptprj*-KO and DKO mice.

I also examined the effects of the DPH treatment on retinal axonal projections in the SC. I intraperitoneally injected DPH (20 mg/kg) into newborn mice daily between P0 and P8, and a focal injection of DiI was performed into the nasal periphery on P8. In vehicle-treated mice, nasal retinal axons formed proper TZs in the posterior SC (Fig. II.11D-H). In contrast, significant proportions of nasal retinal axons of DPH-treated mice formed TZs at more anterior locations within the SC (Fig. 9*I*-*M*): Sagittal sections clearly showed that axons from the nasal retina formed anteriorly shifted TZs in the posterior part of the SC (Fig. II.11G, H, L, M). A quantitative analysis of the distribution of TZs on the SC revealed that the TZs of DPH-treated mice had significantly shifted more anteriorly than those in control mice (relative location of TZ

on the SC: control, 1.2 ± 0.1; DPH-treated, 1.7 ± 0.1, $p = 0.004$) (Fig. II.11N). These phenotypes by the DPH treatment were again similar to those observed in *Ptprj*-KO and DKO mice. Therefore, the increased activity of c-Abl kinases in *Ptprj*-KO and DKO mice may be the cause of the abnormal projections of retinal axons observed in mutant mice.

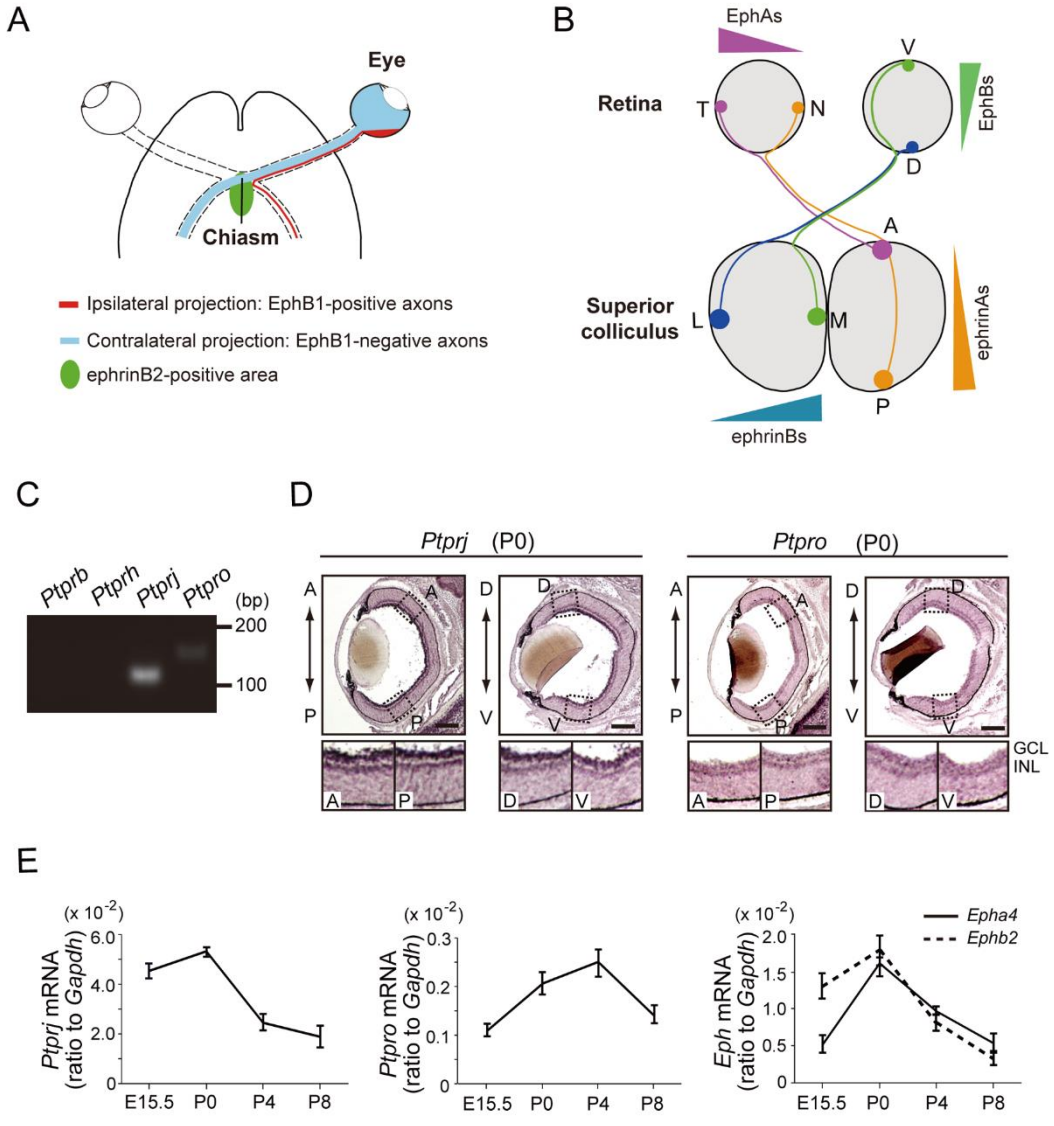
A
Eye
Chiasm
Ipsilateral projection: EphB1-positive axons
Contralateral projection: EphB1-negative axons
ephrinB2-positive area
B
EphAs
Retina
T
N
V
D
EphBs
A
Superior colliculus
L
M
P
ephrinAs
ephrinBs
C
Ptprb
Ptprh
Ptprj
Ptpro
(bp)
200
100
D
Ptprj (P0)
Ptpro (P0)
A
P
D
V
GCL
INL
E
(x 10-2)
Ptprj mRNA (ratio to Gapdh)
Ptpro mRNA (ratio to Gapdh)
Eph mRNA (ratio to Gapdh)
Epha4
Ephb2
E15.5
P0
P4
P8

Figure II.1. Expression of the R3 RPTP subfamily in the developing mouse retina. **A**, Schematic representation of axon guidance of mouse contralateral and ipsilateral RGC axons at the optic chiasm. RGC axons from the ventrotemporal (VT) retinal region express high levels of the EphB1 receptor to sense ephrinB2 at the chiasm and turn ipsilaterally. On the other hand, EphB1-negative RGCs from all other retinal regions project contralaterally. **B**, Schematic representation of the topographic retinocollicular map and expression patterns of Eph receptors and ephrins. Nasal and temporal axons project to the posterior (P) and anterior (A) SC, respectively, while dorsal and ventral retinas are connected to the lateral (L) and medial (M) SC, respectively. Interactions between Eph receptors and ephrins play a pivotal role in the development of the topographic retinocollicular map. N, nasal; T, temporal; D, Dorsal; V, ventral; A, anterior; P, posterior; M, medial; L, lateral. **C**, RT-PCR analyses of the expression of R3 RPTPs in the P0 retina. **D**, Section *in situ* hybridization analyses of *Ptprj* and *Ptpro* in P0 mouse retinas. Anterial-posterial (A-P) and dorsal-ventral (D-V) sections were examined. Lower panels are enlarged images of the regions surrounded by dashed lines in the upper panels. GCL, ganglion cell layer; INL, inner nuclear layer. Scale bars: 250 μm. **E**, Quantitative real-time RT-PCR analyses of the expression of *Ptprj*, *Ptpro*, *Epha4*, and *Ephb2* in the developing retina. The expression of each mRNA was examined by RT-qPCR and shown as relative values to that of *Gapdh* mRNA. Data are shown as the mean ± SEM (n = 3).

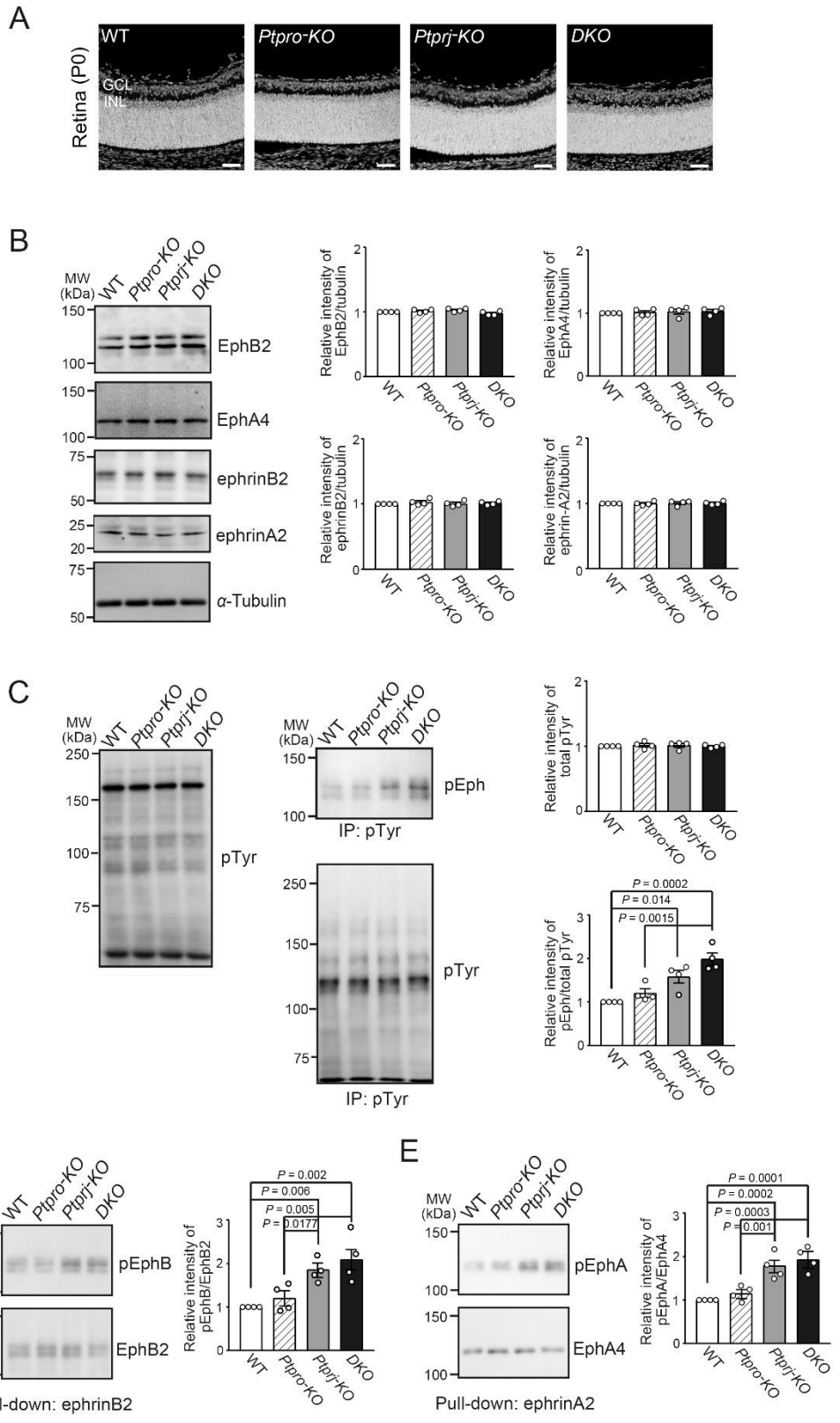
A
WT
Ptpro-KO
Ptprj-KO
DKO
Retina (P0)
GCL
INL
B
MW (kDa)
EphB2
EphA4
ephrinB2
ephrinA2
α-Tubulin
Relative intensity of EphB2/tubulin
Relative intensity of EphA4/tubulin
Relative intensity of ephrinB2/tubulin
Relative intensity of ephrin-A2/tubulin
C
pTyr
IP: pTyr
pEph
Relative intensity of total pTyr
Relative intensity of pEph/total pTyr
P = 0.0002
P = 0.014
P = 0.0015
D
pEphB
EphB2
Pull-down: ephrinB2
Relative intensity of pEphB/EphB2
P = 0.002
P = 0.006
P = 0.005
P = 0.0177
E
pEphA
EphA4
Pull-down: ephrinA2
Relative intensity of pEphA/EphA4
P = 0.0001
P = 0.0002
P = 0.0003
P = 0.001

Figure II.2. Increased tyrosyl phosphorylation of Eph receptors in retinas of *Ptprj*-KO and DKO mice. A, Retinal layering of *Ptpro*-KO, *Ptprj*-KO, and DKO mice. Each retinal section was stained with DAPI. GCL, ganglion cell layer; INL, inner nuclear layer; ONL, outer nuclear layer. Scale bars: 100 μm. **B**, Western blotting of retinal lysates from WT, *Ptpro*-KO, *Ptprj*-KO, and DKO mice with anti-EphA4, anti-EphB2, anti-ephrinA2, anti-ephrinB2, or anti-tubulin antibodies. The right graphs show summaries of relative intensities relative to WT mice (n = 4 per group). **C**, Increased tyrosine phosphorylation of Eph receptors in the retinas of *Ptprj*-KO and DKO mice. Western blotting of lysates with anti-pTyr (left) and anti-pTyr immunoprecipitates with anti-pTyr (middle, lower) and anti-pEph antibodies (middle, upper). The right panel shows a summary of the relative intensity of pEph/total pTyr proteins. **D**, Increased tyrosine phosphorylation of EphB receptors in the retinas of *Ptprj*-KO and DKO mice. EphB receptors were purified by pull-down with ephrinB2-Fc, respectively. Western blotting of pull down samples with anti-pEph antibodies (middle, upper) and anti-EphB1. The right panel shows a summary of the relative intensity of pEph/EphB1 proteins. **E**, Increased tyrosine phosphorylation of EphA receptors in the retinas of *Ptprj*-KO and DKO mice. EphA receptors were purified by pull-down with ephrinA2-Fc. Western blotting of pull down samples with anti-pEph antibodies (middle, upper) and anti-EphA4. The right panel shows a summary of the relative intensity of pEph/EphA4 proteins. Data are shown as the mean ± SEM (n = 4 per group). Sample sizes (n = 3) were calculated from a power analysis, with an effect size of 2.5 (obtained from my pilot experiments), power of 0.8, and significance level of 0.05. Data were analyzed by ANOVA.

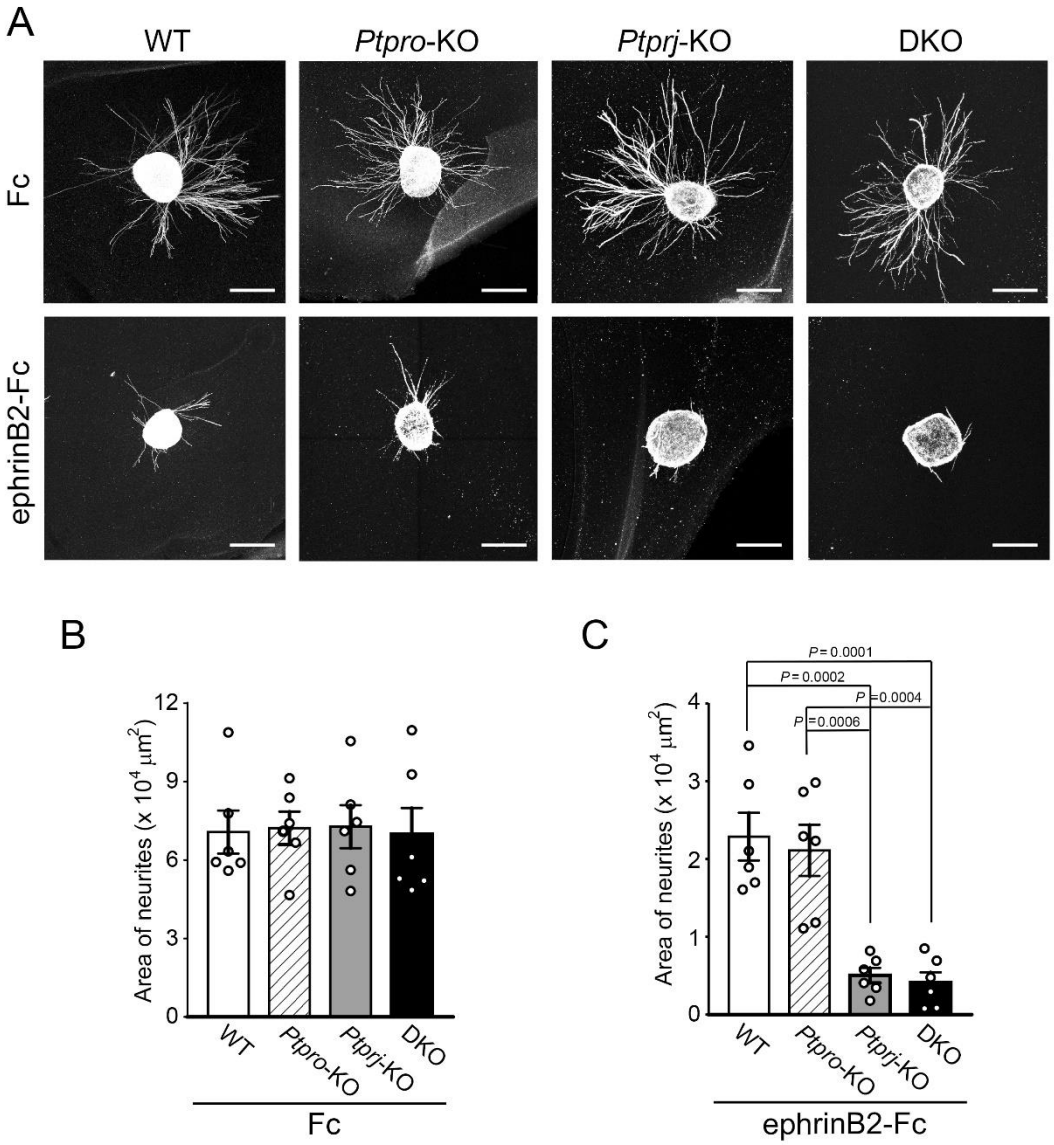
A
WT
Ptpro-KO
Ptprj-KO
DKO
Fc
ephrinB2-Fc
B
Area of neurites (x 10^4 μm^2)
12
9
6
3
0
WT
Ptpro-KO
Ptprj-KO
DKO
Fc
C
P = 0.0001
P = 0.0002
P = 0.0004
P = 0.0006
Area of neurites (x 10^4 μm^2)
4
3
2
1
0
WT
Ptpro-KO
Ptprj-KO
DKO
ephrinB2-Fc

Figure II.3. PTPRJ regulates the sensitivity of retinal axons to ephrinB2. A, Representative images of VT retinal explants prepared from WT, *Ptpro*-KO, *Ptprj*-KO, or DKO mice at E15.5. The explants were cultured for 48 h in collagen gels containing control Fc or ephrinB2-Fc (2 μg/ml each). Scale bars: 500 μm. **B**, **C**, Quantification of the area of neurite outgrowth from the VT explants in collagen gels containing control Fc (**B**) or ephrinB2-Fc (**C**). Values are shown as the mean ± SEM (n = 6 per group). Sample sizes (n = 5) were calculated from a power analysis, with an effect size of 2.5 (obtained from our laboratory pilot experiments), power of 0.8, and significance level of 0.05.

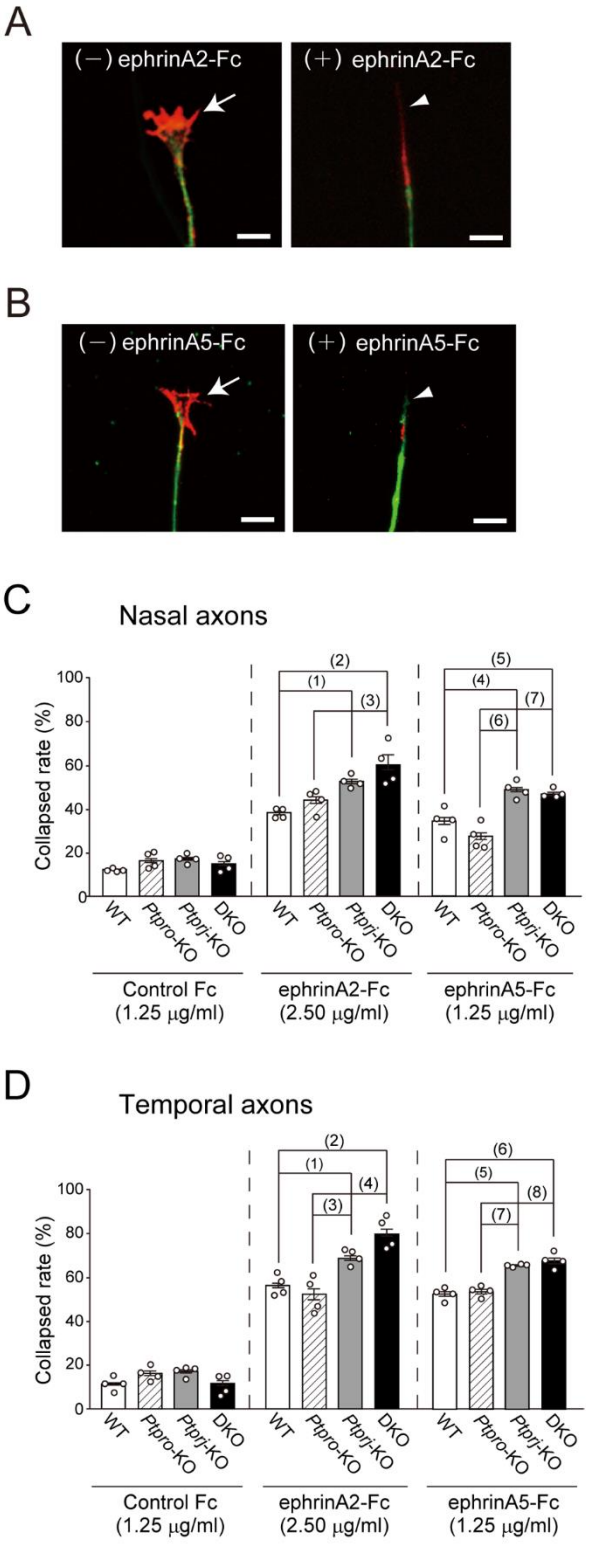
A
(−) ephrinA2-Fc
(+) ephrinA2-Fc
B
(−) ephrinA5-Fc
(+) ephrinA5-Fc
C
Nasal axons
Collapsed rate (%)
100
80
60
40
20
0
(1)
(2)
(3)
(4)
(5)
(6)
(7)
WT
Ptpro-KO
Ptprj-KO
DKO
Control Fc
(1.25 μg/ml)
ephrinA2-Fc
(2.50 μg/ml)
ephrinA5-Fc
(1.25 μg/ml)
D
Temporal axons
Collapsed rate (%)
100
80
60
40
20
0
(1)
(2)
(3)
(4)
(5)
(6)
(7)
(8)
WT
Ptpro-KO
Ptprj-KO
DKO
Control Fc
(1.25 μg/ml)
ephrinA2-Fc
(2.50 μg/ml)
ephrinA5-Fc
(1.25 μg/ml)

Fi**gure II.4.** PTPRJ regulates the sensitivity of retinal axons to ephrinA2 and ephrinA5. Retinal strips prepared from WT, *Ptpro*-KO, *Ptprj*-KO, or DKO mice at E17.5 were cultured for 48 h and then stimulated with ephrinA2-Fc or ephrinA5-Fc for 30 min. Retinal strips with growing axons were stained with anti-βIII tubulin (green) and phalloidin (red). **A**, **B**, Representative morphology of growth cones of WT nasal axons before (-) and after (+) a stimulation with ephrinA2-Fc (2.50 μg/ml) (**A**), or ephrinA5-Fc (1.25 μg/ml) (**B**). Retinal strips with growing axons were stained with anti-βIII tubulin (green) and phalloidin (red). Scale bars: 10 μm. **C**, **D**, Growth cone collapse rates of nasal (**C**) and temporal (**D**) retinal axons after stimulation with control Fc (1.25 mg/ml), ephrinA2-Fc (2.50 mg/ml), or ephrinA5-Fc (1.25 mg/ml). Values are shown as the mean ± SEM (n = 4 per group). *P* values in (**C**): (1), 0.008; (2), 0.0003; (3), 0.002; (4), 0.010; (5), 0.032; (6), 0.0003; (7), 0.0008. *P* values in (**D**): (1), 0.047; (2), 0.00004; (3), 0.005; (4), 0.00003; (5), 0.003; (6), 0.0007; (7), 0.005; (8), 0.001. Sample sizes (n = 3) were calculated from a power analysis, with an effect size of 2.5 (obtained from our laboratory pilot experiments), power of 0.8, and significance level of 0.05. Data were analyzed by ANOVA.

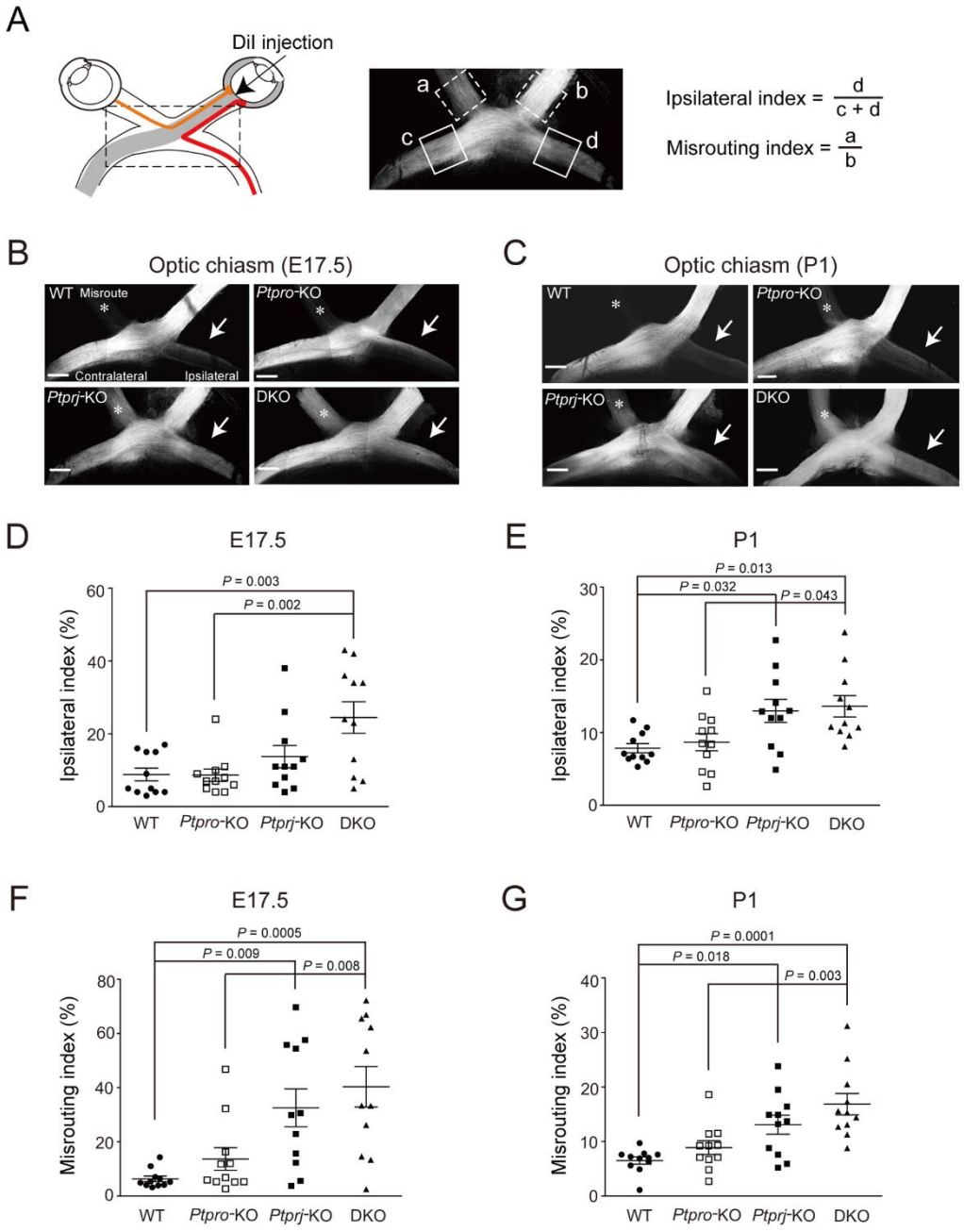
A
DiI injection
a
b
c
d
Ipsilateral index = d / (c + d)
Misrouting index = a / b
B
Optic chiasm (E17.5)
WT Misroute
Contralateral
Ipsilateral
Ptpro-KO
Ptprj-KO
DKO
C
Optic chiasm (P1)
WT
Ptpro-KO
Ptprj-KO
DKO
D
E17.5
Ipsilateral index (%)
P = 0.003
P = 0.002
WT
Ptpro-KO
Ptprj-KO
DKO
E
P1
Ipsilateral index (%)
P = 0.013
P = 0.032
P = 0.043
WT
Ptpro-KO
Ptprj-KO
DKO
F
E17.5
Misrouting index (%)
P = 0.0005
P = 0.009
P = 0.008
WT
Ptpro-KO
Ptprj-KO
DKO
G
P1
Misrouting index (%)
P = 0.0001
P = 0.018
P = 0.003
WT
Ptpro-KO
Ptprj-KO
DKO

Figure II.5. Ipsilateral projections of retinal axons at the OC in WT, *Ptpro*-KO, *Ptprj*-KO, and DKO mice. A, Schematic representation of DiI tracing of retinal axons and quantification of the projection index to the ipsilateral side or contralateral eye. Retinal axons in the right eye were anterogradely labeled with DiI. Axons projected ipsilaterally and misrouted to the contralateral eyes are indicated by a red and orange lines, respectively. The ipsilateral index was calculated by dividing the fluorescent intensity of the ipsilateral optic tract by the total fluorescent intensity of both tracts. The misrouting index was calculated as the ratio between the fluorescent intensity of the left optic nerve and that of the right optic nerve. **B**, **C**, Representative whole-mount ventral view of retinal axons at the OC of WT, *Ptpro*-KO, *Ptprj*-KO, and DKO mice. Retinal axons in the right eye were labeled with DiI at E17.5 (**B**) and P1 (**C**). Arrows and asterisks indicate projections to the ipsilateral side and contralateral optic nerve, respectively. Scale bars: 200 μm. **D**, **E**, Index of projections to the ipsilateral side (n = 11 for each group). **F**, **G**, Index of projections to the contralateral optic nerve (n = 11 for each group). Sample sizes (n = 9) were calculated from a power analysis, with an effect size of 1.3 (obtained from our laboratory pilot experiments), power of 0.8, and significance level of 0.05.

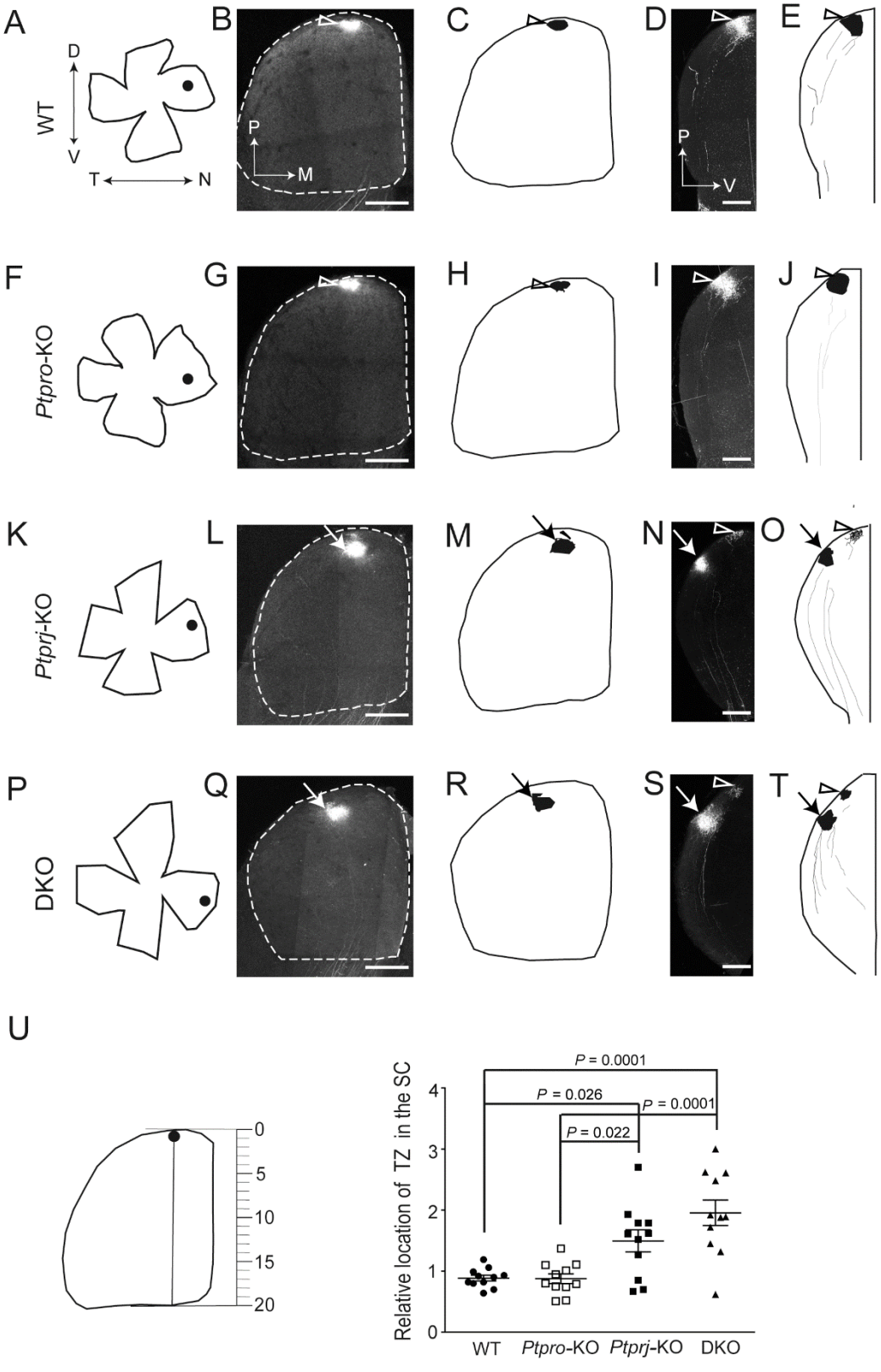
A
B
C
D
E
WT
D
V
T
N
P
M
P
V
F
G
H
I
J
Ptpro-KO
K
L
M
N
O
Ptprj-KO
P
Q
R
S
T
DKO
U
0
5
10
15
20
P = 0.0001
P = 0.026
P = 0.0001
P = 0.022
Relative location of TZ in the SC
4
3
2
1
0
WT
Ptpro-KO
Ptprj-KO
DKO

Figure II.6. Projections of nasal retinal axons to the SC in WT, *Ptpro*-KO, *Ptprj*-KO, and DKO mice. Two days after a focal injection of DiI into the nasal periphery of the right retina on P8, DiI-labeled axons on the SC were analyzed. **A**, **F**, **K**, **P**, Schematic drawings of flat-mount right retinas. The locations of the DiI label in the right retina are indicated by dots. N, nasal; D, dorsal. **B**, **G**, **L**, **Q**, Whole-mount dorsal views of the left SC (posterior up, anterior down). Projection patterns in WT and *Ptpro*-KO mice revealed that nasal retinal axons form TZs at a posterior position (**B**), (**G**), whereas the projections of retinal axons in *Ptprj*-KO and DKO mice showed that the TZs of nasal axons anteriorly shifted (**L**), (**Q**). White dotted lines outline the SC. P, posterior; M, medial. **C**, **H**, **M**, **R**, Schematic drawings of (**B**), (**G**), (**L**), and (**Q**), respectively. **D**, **I**, **N**, **S**, Sagittal sections of the SC along the dotted lines in (**B**), (**G**), (**L**), and (**Q**), respectively. In WT and *Ptpro*-KO mice, TZs were normal (arrowheads). In contrast, in *Ptprj*-KO and DKO mice, large numbers of nasal axons formed anteriorly shifted TZs (arrows) in addition to the normal TZs (arrowheads). P, posterior; V, ventral. **E**, **J**, **O**, **T**, Schematic drawings of (**D**), (**I**), (**N**), and (**S**), respectively. **U**, Analysis of the location of TZs in the SC of WT, *Ptpro*-KO, *Ptprj*-KO, and DKO mice. The center of fluorescence (center of TZs) for each image was used to define the position of the TZ in the SC along the antero-posterior axis. The position ranges between 0 and 20 (left). The right graph shows a summary of the location of TZs. Sample sizes (n = 10 each) were calculated from power analysis, with an effect size of 1.2 (obtained from our laboratory pilot experiments), power of 0.8, and significance level of 0.05. Data were analyzed by ANOVA. Scale bars: 600 μm for (**B**), (**G**), (**L**), (**Q**), and 200 μm for (**D**), (**I**), (**N**), (**S**).

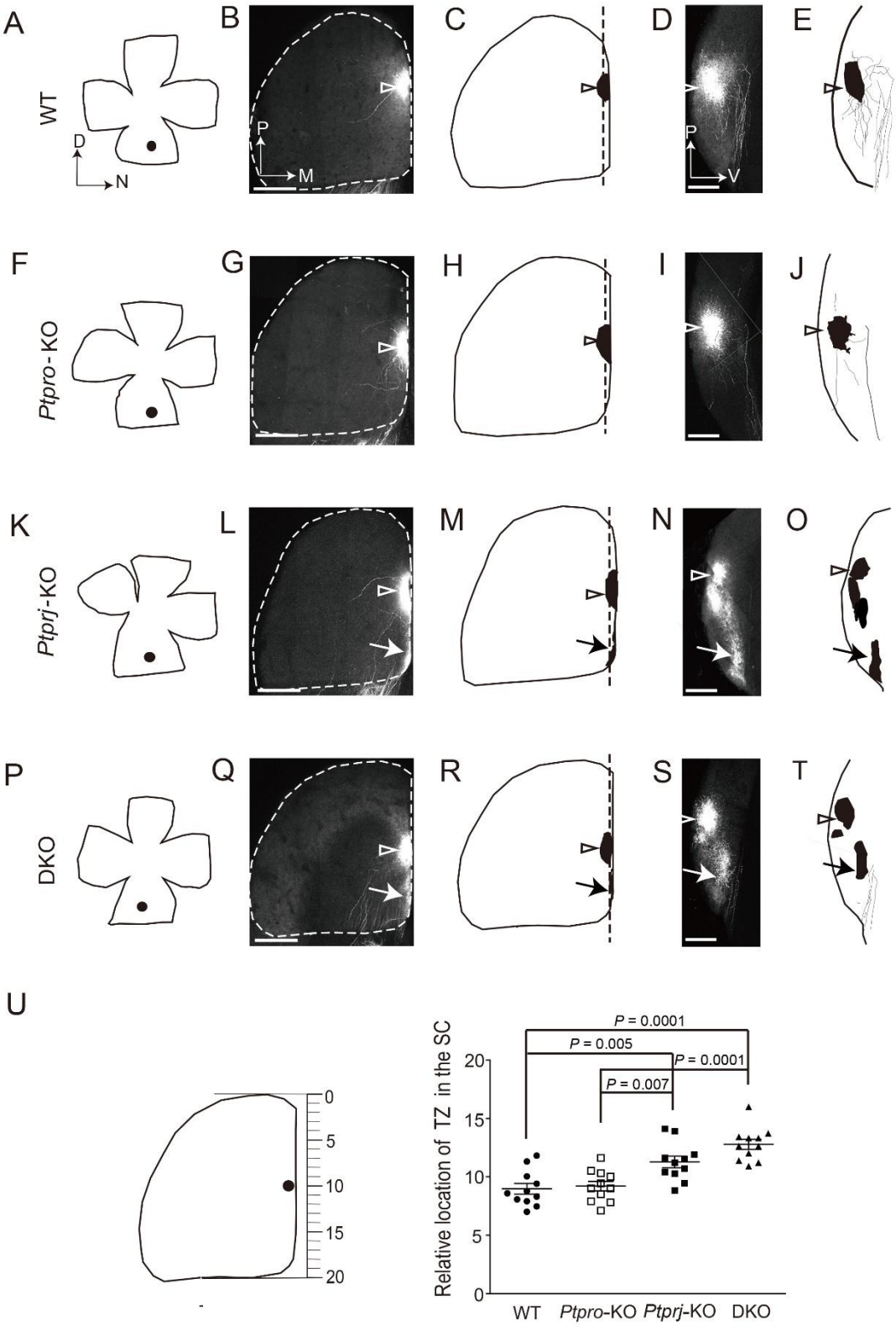
A
WT
D
N
B
P
M
C
D
P
V
E
F
Ptpro-KO
G
H
I
J
K
Ptprj-KO
L
M
N
O
P
DKO
Q
R
S
T
U
0
5
10
15
20
P = 0.0001
P = 0.005
P = 0.0001
P = 0.007
Relative location of TZ in the SC
20
15
10
5
0
WT
Ptpro-KO
Ptprj-KO
DKO

Figure II.7. Projections of ventral retinal axons to the SC in WT, *Ptpro*-KO, *Ptprj*-KO, and DKO mice. Two days after a focal injection of DiI into the ventral periphery of the right retina on P8, DiI-labeled axons on the SC were analyzed. **A**, **F**, **K**, **P**, Schematic drawings of flat-mount right retinas. The locations of the DiI label in the right retina are indicated by dots. N, nasal; D, dorsal. **B**, **G**, **L**, **Q**, Whole-mount dorsal views of the left SC (posterior up, anterior down). Projection patterns in the WT and *Ptpro*-KO mice exhibited that nasal retinal axons form TZs at a posterior position (**B**), (**G**), whereas the projections of retinal axons in *Ptprj*-KO and DKO mice showed that the TZs of ventral axons anteriorly shifted (**L**), (**Q**). White dotted lines outline the SC. P, posterior; M, medial. **C**, **H**, **M**, **R**, Schematic drawings of (**B**), (**G**), (**L**), and (**Q**), respectively. **D**, **I**, **N**, **S**, Sagittal sections of the SC along the dotted lines in (**B**), (**G**), (**L**), and (**Q**), respectively. In WT and *Ptpro*-KO mice, TZs were normal (arrowheads). In contrast, in *Ptprj*-KO and DKO mice, large numbers of ventral axons formed anteriorly shifted TZs (arrows) in addition to the normal TZs (arrowheads). P, posterior; D, dorsal. **E**, **J**, **O**, **T**, Schematic drawings of (**D**), (**I**), (**N**), and (**S**), respectively. **U**, Analysis of the location of TZs in the SC of WT, *Ptpro*-KO, *Ptprj*-KO and DKO mice. The center of fluorescence (center of TZs) for each image was used to define the position of the TZ in the SC along the antero-posterior axis. The position ranges between 0 and 20 (left). The right graph shows a summary of the location of TZs. Sample sizes (n = 10 each) were calculated from a power analysis, with an effect size of 1.2 (obtained from our laboratory pilot experiments), power of 0.8, and significance level of 0.05. Data were analyzed by ANOVA. Scale bars: 600 μm for (**B**), (**G**), (**L**), (**Q**), and 200 μm for (**D**), (**I**), (**N**), (**S**).

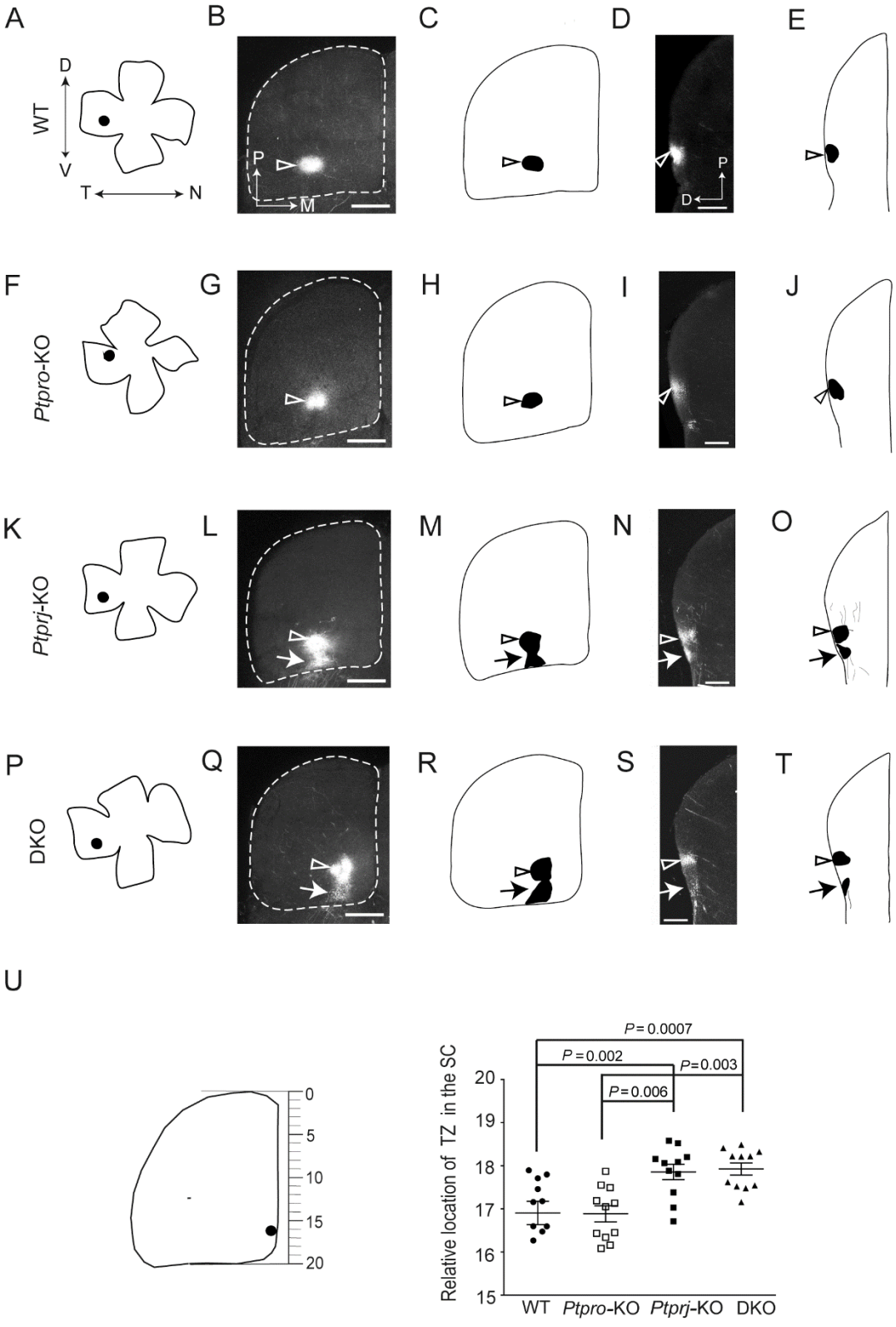
A
B
C
D
E
WT
D
V
T
N
P
M
P
D
F
G
H
I
J
Ptpro-KO
K
L
M
N
O
Ptprj-KO
P
Q
R
S
T
DKO
U
0
5
10
15
20
P = 0.0007
P = 0.002
P=0.003
P = 0.006
Relative location of TZ in the SC
20
19
18
17
16
15
WT
Ptpro-KO
Ptprj-KO
DKO

Figure II.8. Projections of centrotemporal retinal axons to the SC in WT, *Ptpro*-KO, *Ptprj*-KO, and DKO mice. Two days after a focal injection of DiI into the centrotemporal region of the right retina on P8, DiI-labeled axons on the SC were analyzed. **A**, **F**, **K**, **P**, Schematic drawings of flat-mount right retinas. The locations of the DiI label in the right retina are indicated by dots. N, nasal; D, dorsal. **G**, **L**, **Q**, Whole-mount dorsal views of the left SC (posterior up, anterior down). Projection patterns in the WT and *Ptpro*-KO mice exhibited that centrotemporal retinal axons form TZs at a posterior position (**B**), (**G**), whereas the projections of retinal axons in *Ptprj*-KO and DKO mice showed that the TZs of ventral axons anteriorly shifted (**L**), (**Q**). White dotted lines outline the SC. P, posterior; M, medial. **C**, **H**, **M**, **R**, Schematic drawings of (**B**), (**G**), (**L**), and (**Q**), respectively. **D**, **I**, **N**, **S**, Sagittal sections of the SC along the dotted lines in (**B**), (**G**), (**L**), and (**Q**), respectively. In WT and *Ptpro*-KO mice, TZs were normal (arrowheads). In contrast, in *Ptprj*-KO and DKO mice, large numbers of centrotemporal axons formed anteriorly shifted TZs (arrows) in addition to the normal TZs (arrowheads). P, posterior; D, dorsal. **E**, **J**, **O**, **T**, Schematic drawings of (**D**), (**I**), (**N**), and (**S**), respectively. **U**, Analysis of the location of TZs in the SC of WT, *Ptpro*-KO, *Ptprj*-KO and DKO mice. The center of fluorescence (center of TZs) for each image was used to define the position of the TZ in the SC along the antero-posterior axis. The position ranges between 0 and 20 (left). The right graph shows a summary of the location of TZs. Sample sizes (n = 10 each) were calculated from a power analysis, with an effect size of 1.2 (obtained from our laboratory pilot experiments), power of 0.8, and significance level of 0.05. Data were analyzed by ANOVA. Scale bars: 600 μm for (**B**), (**G**), (**L**), (**Q**), and 200 μm for (**D**), (**I**), (**N**), (**S**).

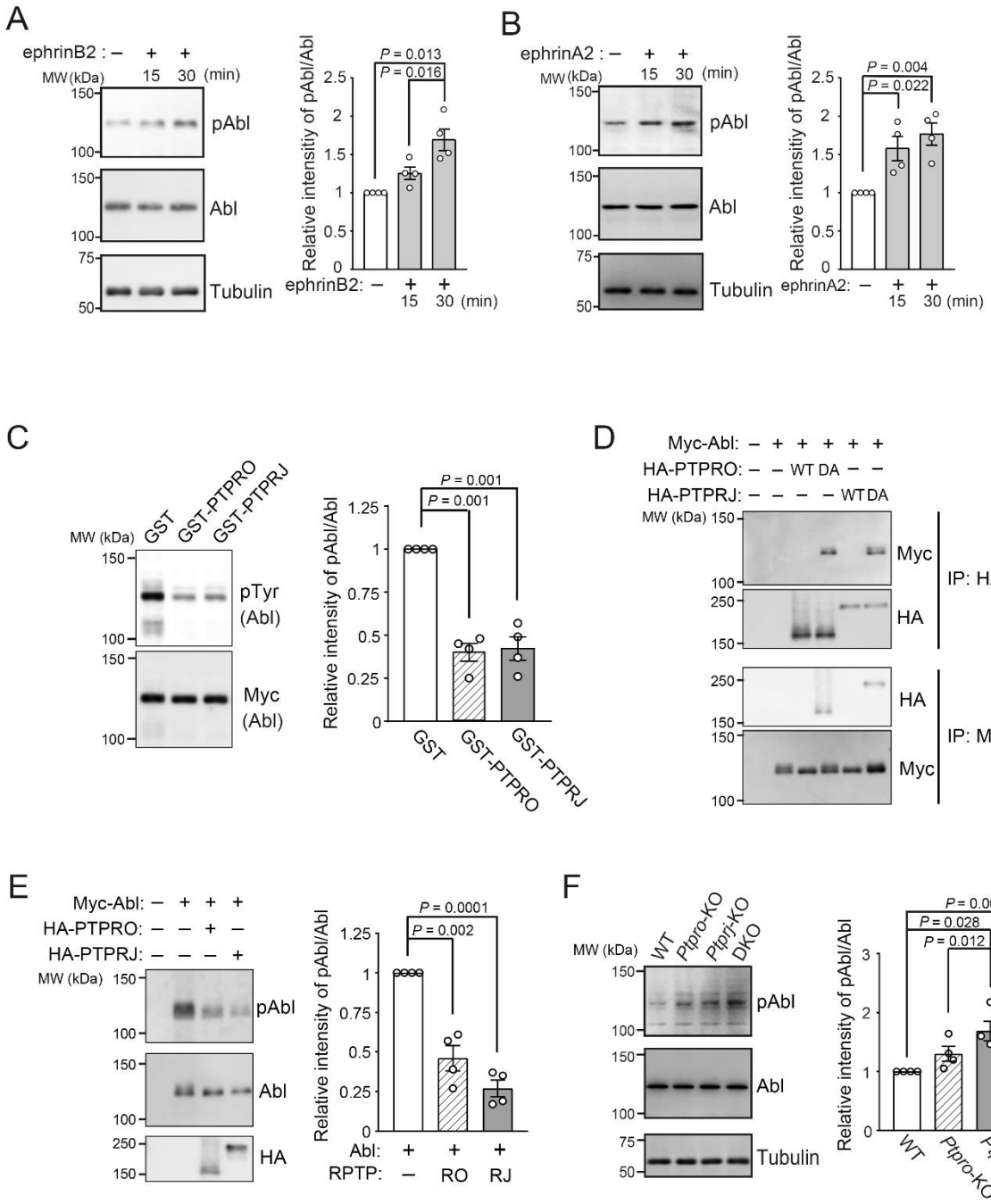
A
ephrinB2 : – + +
MW (kDa) 15 30 (min)
150
100
pAbl
150
100
Abl
75
50
Tubulin
Relative intensity of pAbl/Abl
P = 0.013
P = 0.016
2.5
2
1.5
1
0.5
0
ephrinB2: – + +
15 30 (min)
B
ephrinA2 : – + +
MW (kDa) 15 30 (min)
150
100
pAbl
150
100
Abl
75
50
Tubulin
Relative intensity of pAbl/Abl
P = 0.004
P = 0.022
2.5
2
1.5
1
0.5
0
ephrinA2: – + +
15 30 (min)
C
MW (kDa)
GST
GST-PTPRO
GST-PTPRJ
150
100
pTyr
(Abl)
150
100
Myc
(Abl)
Relative intensity of pAbl/Abl
P = 0.001
P = 0.001
1.25
1
0.75
0.5
0.25
0
GST
GST-PTPRO
GST-PTPRJ
D
Myc-Abl: – + + + + +
HA-PTPRO: – – WT DA – –
HA-PTPRJ: – – – – WT DA
MW (kDa) 150
100
Myc
IP: HA
250
150
HA
250
150
HA
IP: Myc
150
100
Myc
E
Myc-Abl: – + + +
HA-PTPRO: – – + –
HA-PTPRJ: – – – +
MW (kDa) 150
100
pAbl
150
100
Abl
250
150
HA
Relative intensity of pAbl/Abl
P = 0.0001
P = 0.002
1.25
1
0.75
0.5
0.25
0
Abl: + + +
RPTP: – RO RJ
F
MW (kDa)
WT
Ptpro-KO
Ptprj-KO
DKO
150
100
pAbl
150
100
Abl
75
50
Tubulin
Relative intensity of pAbl/Abl
P = 0.001
P = 0.028
P = 0.012
3
2
1
0
WT
Ptpro-KO
Ptprj-KO
DKO

Figure II.9. Increased tyrosine phosphorylation of c-Abl in retinas of *Ptprj*-KO and DKO mice. **A**, Western blotting of cell lysates prepared from dissociated retinal cells treated with or without ephrinB2-Fc (2 μg/ml) for 15 or 30 mins. The antibodies used are shown on the right. A summary of the relative ratio of pAbl/Abl is shown on the right side (n = 4). **B**, Western blotting of cell lysates prepared from dissociated retinal cells treated with or without ephrinA2-Fc (1.5 μg/ml) for 15 or 30 mins. The antibodies used are shown on the right. A summary of the relative ratio of pAbl/Abl is shown on the right side (n = 4). **C**, *In vitro* dephosphorylation assay of the c-Abl protein by PTPRO or PTPRJ. Tyrosine-phosphorylated Myc-c-Abl proteins were incubated with GST, GST-PTPRO, or GST-PTPRJ. After the reaction, c-Abl proteins were analyzed with anti-phosphotyrosine (pTyr) and anti-Myc antibodies. The right graph is a summary of the ratio of pAbl/Abl (n = 4). **D**, Coimmunoprecipitation of c-Abl with the substrate-trapping (DA) mutant of PTPRO or PTPRJ. A Myc-tagged c-Abl expression construct was co-transfected with the control empty vector or expression construct of HA-tagged PTPRO-WT, PTPRO-DA mutant, PTPRJ-WT, or PTPRJ-DA mutant in HEK293T cells. The immunoprecipitation was performed using an anti-HA or anti-Myc antibody. The immunoprecipitates were analyzed with anti-HA and anti-Myc antibodies by Western blotting. **E**, Dephosphorylation of c-Abl by PTPRO and PTPRJ in HEK293T cells. A Myc-tagged c-Abl expression construct was co-transfected with a control empty vector or expression construct of HA-tagged PTPRO-WT or PTPRJ-WT in HEK293T cells. Cell lysates were analyzed with the indicated antibodies by Western blotting. The right graph is a summary of the relative ratio of pAbl/Abl (n = 4). **F**, Increased tyrosine phosphorylation of c-Abl in the retinas of *Ptprj*-KO and DKO mice. Retinal lysates were prepared from WT, *Ptpro*-KO, *Ptprj*-KO, and DKO mice with the indicated antibodies. The right panel shows a summary of the relative

ratio of pAbl/Abl. Values are shown as the mean ± SEM (n = 4). Sample sizes (n = 3) were calculated from a power analysis, with an effect size of 2.5 (obtained from our laboratory pilot experiments), power of 0.8, and significance level of 0.05. Data were analyzed by a one-way ANOVA.

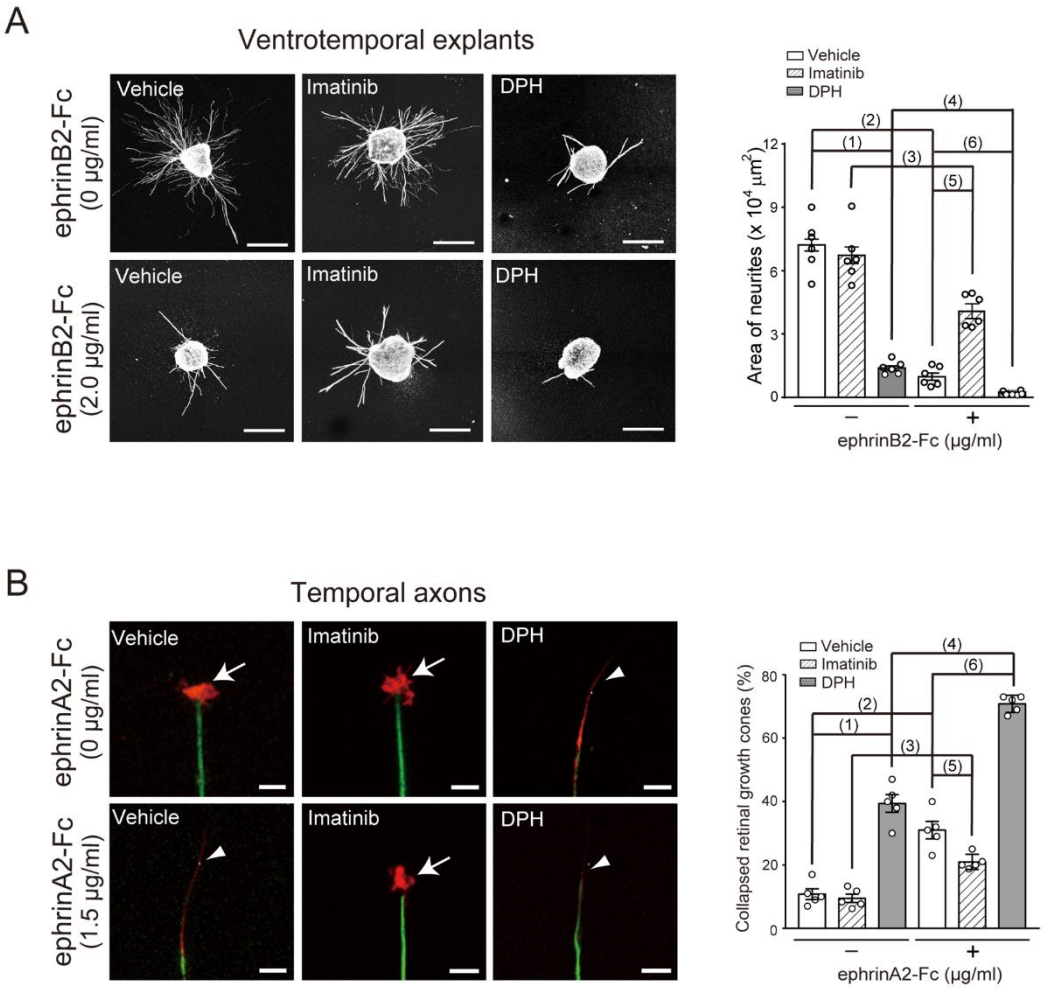
A
Ventrotemporal explants
Vehicle
Imatinib
DPH
ephrinB2-Fc (0 µg/ml)
ephrinB2-Fc (2.0 µg/ml)
Vehicle
Imatinib
DPH
Area of neurites (x 10^4 µm^2)
ephrinB2-Fc (µg/ml)
B
Temporal axons
ephrinA2-Fc (0 µg/ml)
ephrinA2-Fc (1.5 µg/ml)
Collapsed retinal growth cones (%)
ephrinA2-Fc (µg/ml)

Figure II.10. Ephrin signaling is partially mediated by c-Abl in the retina. **A**, Effects of imatinib and DPH on the inhibition of neurite outgrowth from ventrotemporal retinal explants by ephrinB2-Fc. Representative images of VT retinal explants cultured for 48 h in collagen gels containing imatinib (10 μg/ml) or DPH (20 μg/ml) with or without ephrinB2-Fc (2 μg/ml) (the left panels). Scale bars: 500 μm. A summary of the quantification of the area of neurite outgrowth is shown on the right side. Values are shown as the mean ± SEM (n = 6 per group). *P* values: (1), 0.000003; (2), 0.000001; (3), 0.00003: (4), 0.035; (5), 0.000001; (6), 0.047. **B**, Effects of imatinib and DPH on retinal growth cone collapse induced by ephrinA2-Fc. Morphology of temporal retinal growth cones, which were treated with imatinib (10 μg/ml), DPH (20 μg/ml), or vehicle for 30 min. They were then reacted with or without ephrinA2-Fc (1.5 μg/ml). A summary of the quantification of growth cone collapse is shown on the right side. Values are shown as the mean ± SEM (n = 4). *P* values: (1), 0.0001; (2), 0.001; (3), 0.0001: (4), 0.001; (5), 0.014; (6), 0.001. Sample sizes were calculated from a power analysis, with an effect size of 2.5 (obtained from our laboratory pilot experiments), power of 0.8, and significance level of 0.05. Data were analyzed by ANOVA.

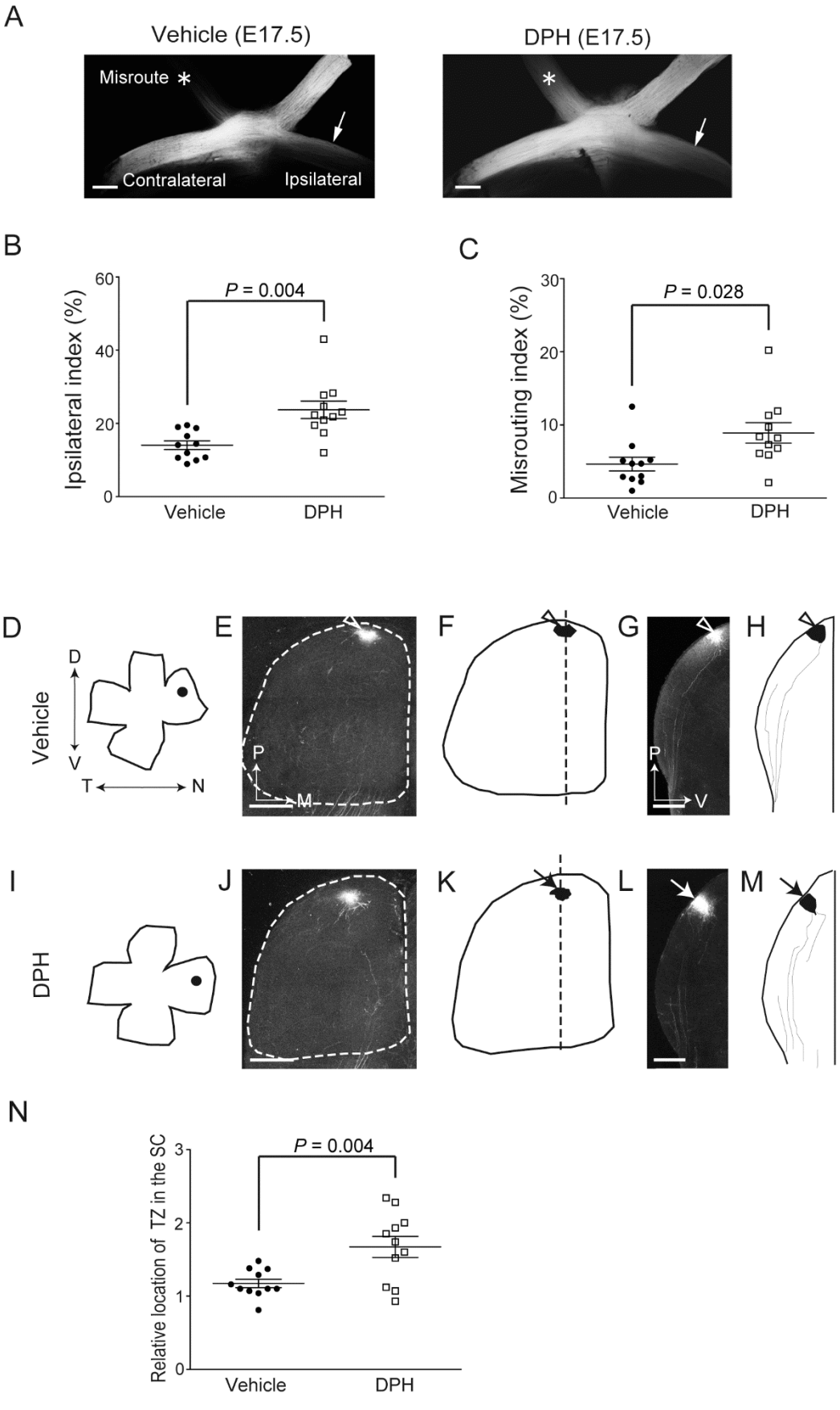
A
Vehicle (E17.5)
DPH (E17.5)
Misroute
Contralateral
Ipsilateral
B
Ipsilateral index (%)
P = 0.004
Vehicle
DPH
C
Misrouting index (%)
P = 0.028
Vehicle
DPH
D
Vehicle
D
V
T
N
E
P
M
F
G
P
V
H
I
DPH
J
K
L
M
N
Relative location of TZ in the SC
P = 0.004
Vehicle
DPH

Figure II.11. Aberrant activation of c-Abl leads to impaired retinal axonal projections. **A**, Whole-mount ventral views of projections at the OC in vehicle or DPH-treated mice. Pregnant C57BL/6 mice were treated with DMSO (vehicle) or DPH (20 mg/kg) daily from E12.5 to E16.5, and retinal axons in the right eye were then labeled with DiI at E17.5. Scale bars: 200 μm. Arrows and asterisks indicate projections to the ipsilateral side and opposite retina, respectively. **B**, Index of misrouting to the ipsilateral side in DPH-treated mice (n = 11 for each group). **C**, Index of misrouting to the contralateral retina in DPH-treated mice (n = 11 for each group). **D**, **I**, Schematic drawings of flat-mount right retinas. DMSO or DPH（20 mg/kg） was injected into mice daily between P0 and P8. A focal injection of Dil into the nasal periphery of the right retina was performed on P8, and the location of DiI in the retina and SC was analyzed on P10. The locations of the DiI label in the nasal periphery of the right retina are indicated by dots. Nasal axons to the right and dorsal axons to the top. N, nasal; D, dorsal. **E**, **J**, Representative whole-mount ventral views of SC. P, posterior; M, medial. **F**, **K**, Schematic drawings of (**E**) and (**J**), respectively. Sagittal sections were prepared along the indicated lines. **G**, **L**, Sagittal sections of the SC in (**E**) and (**J**), respectively. A normal TZ was observed in the control mouse (arrowhead). In contrast, large numbers of nasal axons formed an anteriorly shifted TZ in the DPH-treated mouse (arrow). P, posterior; V, ventral. **H**, **M**, Schematic drawings of (**G**) and (**L**), respectively. **N**, Quantitative analysis of the location of TZs in control and DPH-treated mice (n = 11 for each group). Sample sizes (n = 10) were calculated from a power analysis, with an effect size of 2.5 (obtained from our laboratory pilot experiments), power of 0.8, and significance level of 0.05. Scale bars: 600 μm for (**E**), (**J**) and 200 μm for (**G**), (**L**).

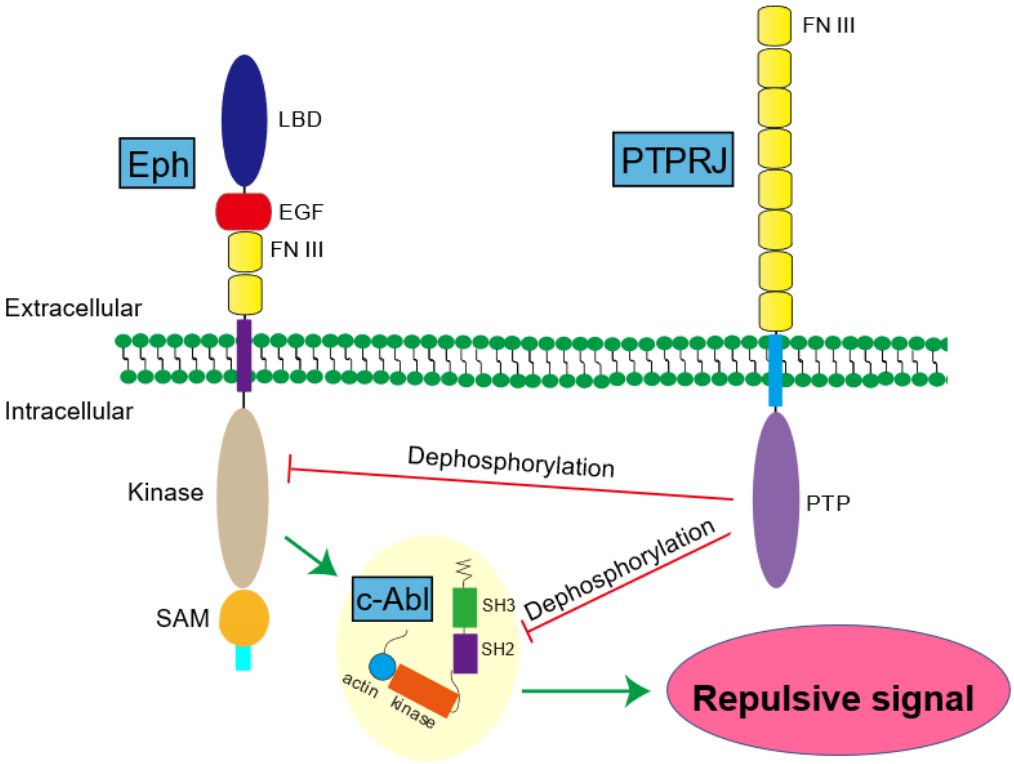
FN III
LBD
Eph
PTPRJ
EGF
FN III
Extracellular
Intracellular
Dephosphorylation
Kinase
PTP
c-Abl
SH3
Dephosphorylation
SAM
SH2
actin
kinase
Repulsive signal

Figure II.12. A schematic picture shows the negatively regulation of PTPRJ in Eph signaling. PTPRJ plays critical roles in retinal axonal projections through the control of Eph and c-Abl activities. c-Abl is downstream of ephrin-Eph signaling in retinal axons. PTPRJ suppresses c-Abl activity as well as Eph receptors activity. Imatinib is an Abl kinase inhibitor, DPH is Abl kinase activator.

Discussion

Retinocollicular projections are a good model for elucidating the mechanisms underlying axon guidance and topographic map formation (Brown A et al., 2000, Carreres MI et al., 2001; Feldheim DA et al., 2004). In this study, I demonstrated that PTPRJ are required for retinal axon guidance at the OC and retinocollicular map formation in mice. PTPRJ are strongly expressed in RGCs at appropriate developmental stages to regulate guidance and mapping (Fig. II.1). I found that the phosphorylation levels of EphA and EphB receptors were up-regulated in the retinas of *Ptprj*-KO and DKO mice (Fig. II.2). The retinal axons of *Ptprj*-KO and DKO mice showed an enhanced response to ephrinA2 and ephrinB2 proteins in growth cone collapse assays (Fig. II.4) and neurite extension assays (Fig. II.3), respectively. These results suggested that ephrin-Eph repulsive signaling was upregulated in *Ptprj*-KO and DKO mice. Consistent with these results, axon tracing analyses *in vivo* revealed that the proportion of RGC axons that misrouted to the ipsilateral side or to the opposite eye through the OC was greater in *Ptprj*-KO mice and DKO mice than in WT mice (Fig. II.5). These projection phenotypes at the OC are explained by the following mechanisms: axons with EphB activities higher than a certain level receive hyper-repulsive signals, avoid the midline chiasm expressing ephrinB2 and project ipsilaterally or to the contralateral eye. Furthermore, the nasal, ventral, and centrotemporal retinal axons of *Ptprj*-KO and DKO mice commonly exhibited abnormal projections in which they made ectopic TZs anteriorly shifted in the SC (Figs. II.6-8). These abnormal projections are explained by the mechanism that EphA receptors in *Ptprj*-deficient RGC axons had an enhanced response to ephrinAs in the SC due to the lack of suppression by PTPRJ.

In addition, I revealed that PTPRJ dephosphorylated c-Abl located downstream of Eph receptors (Figs.II.9 and II.10). I demonstrated that PTPRJ recognized c-Abl as a substrate and dephosphorylated it in HEK293T cells (Fig. II.9C-E). The phosphorylation levels of c-Abl were consistently up-regulated in the retinas of *Ptprj*-KO and DKO mice (Fig. II.9E). Ephrin-Eph signaling is reportedly mediated by c-Abl kinase in some cell types (Chang et al., 2008, Genander et al., 2009). In this study, I found that c-Abl was activated in the retinal cells following a stimulation with ephrinB2 or ephrinA2 (Fig. II.9A, B). The requirement of c-Abl activity for repulsive Eph signaling is clear from my *in vitro* neurite extension assays and collapse assays: the inhibitory effect of ephrinB2 on neurite extension was suppressed by a c-Abl inhibitor (imatinib) and enhanced by a c-Abl activator (DPH) (Fig. II.10A); and ephrinA2-induced collapse was also suppressed by imatinib and enhanced by DPH (Fig. II.10B). Furthermore, I also demonstrated that the proportion of RGC axons that misrouted to the ipsilateral side or to the opposite eye through the OC was increased in DPH-treated animals, suggesting that repulsive ephrinB-EphB signaling is upregulated by DPH. Nasal retinal injections of DiI showed that c-Abl was involved in the appropriate topographic mapping of RGC axons in the SC. In mice treated with DPH, nasal axons aberrantly terminated, anterior to the appropriate position in the SC (Fig. II.11). This anterior shift is expected if repulsive signaling by EphA along the A-P axis in the SC is enhanced by the activation of c-Abl. Collectively, these results indicate that PTPRJ suppress ephrin-Eph-c-Abl repulsive signaling in the RGC axons of mice through the dephosphorylation of both Eph and c-Abl kinases.

Previous studies that analyzed retinocollicular projections in *EphB*-deficient mice indicated that EphBs are necessary for topographic map formation along the medio-lateral (M-L) axis (Hindges et al., 2002; Thakar et al., 2011). However, there were no

alterations in retinal axonal projections along the M-L axis in the SC of all genotypes. However, there was no alterations in RGC axon projections along the M-L axis in the SC of all genotypes. Therefore, these results indicate that c-Abl is required for the transduction of repulsive signals but not attractive signals by Eph receptors in RGC axons. Molecular mechanism for attractive signaling by EphB receptors has not yet been elucidated, but it may differ from that of repulsive signaling by Eph receptors. Here it should be noted that Wnt-Ryk signaling reportedly plays a pivotal role in RGC axonal projections along the M-L axis in the SC (Lim et al., 2010).

Our laboratory previously results showed that PTPRO, but not PTPRJ, dephosphorylated Eph receptors in chicks and that PTPRO plays an important role in retinotectal topographic map formation (Shintani et al., 2006). However, murine R3 RPTP subfamily members (PTPRB, PTPRH, PTPRJ, and PTPRO) equally dephosphorylated Eph receptors as substrates (Sakuraba et al., 2013). I revealed that *Ptpro* and *Ptprj* were expressed in the developing mouse retina (Fig. II.1C). I herein showed that murine PTPRO and PTPRJ equally dephosphorylated Eph receptors and c-Abl in *in vitro* analyses (Figs. II.9C-E). However, the expression level of *Ptpro* was markedly lower than that of *Ptprj*, and the temporal expression profile of *Ptpro* was distinct from those of *Ptprj* and *Ephs* (Fig. II.1*E*). Consistently, I did not detect any evident alterations in the projections of retinal axons in *Ptpro*-KO mice, similar to a previous study (Gatto et al., 2013). I did not detect alterations in the gene expression of *Ptprj* in *Ptpro*-KO mice or *Ptpro* in *Ptprj*-KO mice, which again suggests the small contribution of PTPRO to retinal axonal projections (data not shown). Thus, species differences exist in enzyme-substrate relationships between R3 RPTP subfamily members and Eph receptors: in mouse retinal axons, PTPRJ predominantly regulates repulsive Eph signaling, in contrast to PTPRO in chicks.

It is important to note that PTPRJ dephosphorylates several RPTKs (Sakuraba et al., 2013; Shintani et al., 2015). Alterations in the activities of RPTKs other than Ephs may also contribute to the defects observed in *Ptprj*-KO and DKO mice. The HGF receptor, a substrate of PTPRJ, has been implicated in axon outgrowth (Pante et al., 2005; Sakuraba et al., 2013). I found that the length of axons extending from retinal explants was similar among WT, *Ptprj*-KO, and DKO mice, and there did not appear to be a delay in the arrival of retinal axons at the SC in *Ptprj*-KO and DKO mice (data not shown). These results suggest the absence of general defects in axon outgrowth by *Ptprj*-KO and DKO. On the other hand, PTPRO has been shown to regulate the axonal branching of trigeminal ganglion cells by inhibiting TrkB and Ret signaling (Gatto et al., 2013). TrkB has also been implicated in the regulation of the axonal branching of retinal axons (Marler et al., 2008). However, alterations in the tyrosine phosphorylation level of TrkB were not detected in the retina of *Ptprj*-KO or DKO mice (our laboratory unpublished observations). Nevertheless, PTPRJ may control axonal projections through other signaling pathways. Further studies are needed to identify additional physiological substrates for PTPRJ.

My present results indicated that PTPRJ plays critical roles in retinocollicular projections by controlling the repulsive signal by Eph and c-Abl activities. To the best my knowledge, this is the first study to implicate PTPRJ in axon guidance in mammals. However, ephrin reverse signaling has also been suggested to contribute to topographic retinocollicular map formation, as well as Eph forward signaling (Yates et al. 2001, 2004; Thakar et al., 2011); the Eph-ephrin interaction transduces signals bidirectionally not only into Eph-expressing cells (forward signaling), but into ephrin-expressing cells (reverse signaling). In addition, competition between axons based on repellant interactions plays an important role in mapping (Brown et al. 2000; Yates et al. 2004;

Tsigankov and Koulakov 2006). In this mechanism, the relative rather than absolute levels of EphA forward signaling appears to be important for mapping (Brown et al. 2000; Reber et al. 2004). It currently remains unclear whether PTPRJ is involved in the regulation of ephrin reverse signaling and axonal competitive signaling. The cell type-specific gene targeting of *Ptprj* will contribute to PTPRJ functions in these signals being elucidated in future studies.

References

Alai D, Blake R (1999) Grouping visual features during binocular rivalry, Vision Res. 39, 4341-4353.

Andersen JN, Mortensen OH, Peters GH, Drake PG, Iversen LF, Olsen OH, Jansen PG, Andersen HS, Tonks NK, Moller NP (2001) Structural and evolutionary relationships among protein tyrosine phosphatase domains. Mol Cell Biol 21:7117-7136.

Anderson RB, Walz A, Holt CE, Key (1998) Chondroitin sulfates modulate axon guidance in embryonic Xenopus brain. Dev Biol 202:235-243.

Alonso A, Sasin J, Bottini N, Friedberg I, Osterman A, Godzik A, Hunter T, Dixon J, Mustelin T (2004) Protein tyrosine phosphatases in the human genome. Cell 117:699 711.

Arvanitis D, Davy A (2008) Eph/ephrin signaling: networks. Genes Dev 22: 416–429.

Baumer S, Keller L, Holtmann A, Funke R, August B, Gamp A, Wolburg H, Wolburg-Buchholz K, Deutsch U, and Vestweber D (2006) Vascular endothelial cell-specific phosphotyrosine phosphatase (VE-PTP) activity is required for blood vessel development. Blood 107, 4754–4762

Beltran PJ, Bixby JL, Masters BA (2003) Expression of PTPRO during mouse Development suggests involvement in axonogenesis and differentiation of NT-3 and NGF-dependent neurons. J Comp Neurol 456:384-395.

Brown A, Yates PA, Burrola P, Ortuno D, Vaidya *A,* Jessell TM, Pfaff SL, O'Leary DD, Lemke G (2000) Topographic mapping from the retina to the midbrain is controlled by relative but not absolute levels of EphA receptor signaling. Cell 102:77-88.

Carreres MI, Escalante A, Murillo B, Chauvin G, Gaspar P, Vegar C, Herrera E (2011) Transcription factor foxd1 is required for the specification of the temporal retina in mammals. Neurosci 31:5673-5681.

Cheng HJ, Nakamoto M, Bergemann AD, Flanagan JG (1995) Complementary gradients in expression and binding of ELF-1 and Mek4 in development of the topographic retinotectal projection map. Cell 82:371-381.

Chilton JK (2006). Molecular mechanisms of axon guidance. Dev Biol 292, 13-24

Chang Q, Jorgensen C, Pawson T, Hedley DW (2008) Effects of dasatinib on EphA2 receptor tyrosine kinase activity and downstream signaling in pancreatic cancer. Br J Cancer 99:1074-1082

Connor RJ, Menzel P, Pasquale EB (1998) Expression and tyrosine phosphorylation of Eph receptors suggest multiple mechanisms in patterning of the visual system. Dev Biol 193:21-35.

Dunn DM, Woodford MR, Truman AW, Jensen SM, Schulman J, Caza T, Remillard TC, Loiselle D, Wolfgeher D, Blagg BS, et al. (2015) c-Abl Mediated Tyrosine Phosphorylation of Aha1 Activates Its Co-chaperone Function in Cancer Cells. Cell

Rep. 12:1006-1018.

Fachinger G, Deutsch U, Risau W (1999) Functional interaction of vascular endothelial-protein tyrosine phosphatase with the angiopoietin receptor Tie-2. Oncogene 18:5948-5953.

Feldheim DA, Nakamoto M, Osterfield M, Gale NW, DeChiara TM, Rohatgi R, Yancopoulos GD, Flanagan JG (2004) Loss-of-function analysis of EphA receptors in retinotectal mapping. J Neurosci 24:2542-2550.

Flanagan JG, Vanderhaeghen, P (1998) The ephrins and Eph receptors in neural development. Annu. Rev. Neurosci. 21, 309-345

Flint AJ, Tiganis T, Barford D, Tonks NK (1997) Development of "substrate-trapping" mutants to identify physiological substrates of protein tyrosine phosphatases. Proc. Natl. Acad. Sci. USA. 94:1680-1685.

Gatto G, Dudanova I, Suetterlin P, Davies AM, Drescher U, Bixby JL, Klein R (2013). Protein tyrosine phosphatase receptor type O inhibits trigeminal axon growth and branching by repressing TrkB and Ret signaling. J Neurosci 33:5399-5410.

Gaya A, Pirotto F, Palou E, Autschbach F, Del Pozo V, Sole J, Serra-Pages C (1999) CD148, a new membrane tyrosine phosphatase involved in leukocyte function. Leuk Lymphoma 35:237-243.

Genander M, Halford MM, Xu NJ, Eriksson *M*, Yu Z, Qiu Z, Martling A, Greicius G, Thakar S, Catchpole T, et al (2009) Dissociation of EphB2 signaling pathways mediating progenitor cell proliferation and tumor suppression. Cell 139: 679-692

Godement P, J Vanselow, S Thanos, F Bonhoeffer (1987) A study in developing visual Systems with a new method of staining neurons and their processes in fixed tissue. Development 101:697-713.

Greuber EK, Smith-Pearson P, Wang J, Pendergast AM (1998) Role of ABL family kinases in Flanagan JG, Vanderhaeghen P. The ephrins and Eph receptors in neural development. Annu Rev Neurosci. 21:309–345.

Guillery RW, Mason CA, Taylor JS (1995) Developmental determinants at the mammalian optic chiasm. J Neurosci 15:4727–4737.

Gonzalez-Brito MR, Bixby JL (2009) Protein tyrosine phosphatase receptor type O regulates development and function of the sensory nervous system. 42:458–465.

Harbott LK, Nobes CD (2005) A key role for Abl family kinases in EphA receptor Mediated growth cone collapse. Mol Cell Neurosci 30:1-11.

Himanen JP, Chumley MJ, Lackmann M, Li C, Barton WA, Jeffrey PD, Vearing C, Geleick D, Feldheim DA, Boyd AW, Henkemeyer M, Nikolov DB (2004) Repelling class discrimination: ephrin-A5 binds to and activates EphB2 receptor signaling. Nat Neurosci 7: 501-509.

Hindges R, McLaughlin T, Genoud N, Henkemeyer M, O'Leary DDM (2002) EphB Forward signaling controls directional branch extension and arborization required for dorsal ventral retinotopic mapping. Neuron 35:475-487.

Hornberger MR, Dutting D, Ciossek T, Yamada T, Handwerker C (1999) Modulation of EphA receptor function by coexpressed ephrinA ligands on retinal ganglion cell axons. Neuron 22:731-742.

Sadakata HH, Okazawa T, Sato Y, Supriatna H, Ohnishi S, Kusakari Y, Murata T, Ito U, Nishiyama T, Minegishi A, Harada T, Matozaki (2009) SAP-1 is a microvillus-specific protein tyrosine phosphatase that modulates intestinal tumorigenesis. Genes Cells 14, 295–308

Jeffery G (2001) Architecture of the optic chiasm and the mechanisms that sculpt its development. Physiol Rev 81:1393-1414.

Jeon M, Zinn K (2015) R3 receptor tyrosine phosphatases: conserved regulators of receptor tyrosine kinase signaling and tubular organ development. Semin Cell Dev Biol. 37:119–26.

Johnson KG, Van Vactor D (2003) Receptor protein tyrosine phosphatases in nervous system development. Physiological Reviews 83 1–24.

Klein R (2012) Eph/ephrin signaling during development. Development 139: 4105–4109.

Koleske AJ, Gifford AM, Scott ML, Nee M, Bronson RT, Miczek KA, Baltimore D (1998) Essential role for abl and arg tyrosine kinases in neurulation. Neuron 21:1259-1272.

Kullander K, Klein R (2002) Mechanisms and functions of Eph and ephrin signallingNat Rev Mol Cell Biol. 3:475–486.

Lim BK, Cho SJ, Sumbre G, Poo MM (2010) Region-specific contribution of ephrin B and Wnt signaling to receptive field plasticity in developing optic tectum. Neuron 65:899–911.

Liu T, Zeng X, Sun F, Hou H, Guan Y, Guo D, Ai H, Zhang G, Wang W (2017) EphB4 Regulates self-renewal, proliferation and neuronal differentiation of human embryonic neural stem cells in vitro. Cell Physiol Biochem 41:819-834.

Marcus RC, Gale NW, Morrison ME, Mason CA, Yancopoulos GD (1996) Eph family receptors and their ligands distribute in opposing gradients in the developing mouse retina. Dev Biol 180:786-789.

Marler KJ, Becker-Barroso E, Martínez A, Llovera M, Wentzel C, Poopalasundaram S, Hindges R, Soriano E, Comella J, Drescher U (2008) A TrkB/EphrinA interaction controls retinal axon branching and synaptogenesis. J Neurosci 28:12700-12712.

Mann F, Holt CE (2001) Control of retinal growth and axon divergence at the chiasm: lessons from Xenopus. Bioessays. 23: 319–326.

Matozaki T, Murata Y, Mori M, Kotani T, Okazawa H, Ohnishi H (2010) Expression, localization, and biological function of the R3 subtype of receptor-type protein tyrosine phosphatases in mammals. Cell Signal. 22(12):1811–7.

McLaughlin T, Hindges R, O'Leary DDM (2003a) Regulation of axial patterning of the retina and its topographic mapping in the brain. Curr Opin Neurobiol 13:57-69.

McLaughlin T, Hindges R, Yates PA, O'Leary DDM (2003b) Bifunctional action of ephrin-B1as a repellent and attractant to control bidirectional branch extension in dorsal-ventral retinotopic mapping. Development 130:2407- 2418.

Mclaughlin T, O'Leary DDM (2005) Molecular gradients and development of Retinotopic maps. Annu Rev Neurosci 28:327-355.

Monschau B, Kremoser C, Ohta K, Tanaka H, Kaneko T, Yamada T, Handwerker C, Hornberger MR, Loschinger J, Pasquale EB (1997) Shared and distinct functions Of RAGS and ELF-1 in guiding retinal axons. EMBO J. 16:1258–1267.

Noren NK, Foos G, Hauser CA, Pasquale EB (2006) The EphB4 receptor suppresses breast cancer cell tumorigenicity through an Abl-Crk pathway. Nat Cell Biol 8:815-825.

Pante G, Thompson J, Lamballe F, Iwata T, Ferby I, Barr FA, Davies AM, Maina F, Klein R (2005) Mitogen-inducible gene 6 is an endogenous inhibitor of HGF/Met induced cell migration and neurite growth. J Cell Biol 171:337-348.

Pasquale EB (2005) Eph receptor signaling casts a wide net on cell behavior. Nat Rev Mol Cell Biol 6:462–475

Petros TJ, Rebsam A, Mason CA (2008) Retinal axon growth at the optic chiasm: to cross or not to cross. Annu Rev Neurosci. 31:295–315.

Plump AS, Erskine L, Sabatier C, Brose K, Epstein C.J, Goodman C.S, Mason C.A, Tessier Lavigne M (2002) Slit1 and Slit2 cooperate to prevent premature midline crossing of retinal axons in the mouse visual system. Neuron 33:219-232.

Reber M, Burrola P, Lemke G (2004) A relative signalling model for the formation of a Topographic neural map. Nature 431:847-853.

Sadakata H, Okazawa H, Sato T, Supriatna Y, Ohnishi H, Kusakari S, Murata Y, Ito T, Sakuraba J, Shintani T, Tani S, Noda M (2013) Substrate specificity of R3 receptor-like Protein tyrosine phosphatase subfamily toward receptor protein-tyrosine kinases. J Biol Chem 288:23421-23431.

Sakuta H, Takahashi H, Shintani T, Etani K, Aoshima A, Noda M (2006) Role of bone morphogenic protein 2 in retinal patterning and retinotectal projection. J Neurosci 26: 10868-10878.

Sefton BM, Hunter T, Raschke WC (1981) Evidence that the Abelson virus protein functions in vivo as a protein kinase which phosphorylates tyrosine. Proc. Natl. Acad. Sci. U.S.A 78, 1552-1556.

Shintani T, Ihara M, Sakuta H, Takahashi H, Watakabe I, Noda M (2006) Eph receptors are negatively controlled by protein tyrosine phosphatase receptor type O. Nat Neurosci 9:761-769.

Shintani T, Ihara M, Tani S, Sakuraba J, Sakuta H, Noda M (2009) APC2 plays an essential role in axonal projections through the regulation of microtubule stability. J Neurosci 29:11628-11640.

Shintani T, Higashi S, Takeuchi Y, Gaudio E, Trapasso F, Fusco A, Noda M (2015) The R3 receptor-like protein tyrosine phosphatase subfamily inhibits insulin signalling by dephosphorylating the insulin receptor at specific sites. J Biochem 158:235-243.

Simon, DK, O'Leary DDM (1992) Development of topographic order in the mammalia retinocollicular projection. J Neurosci 12:1212-1232.

Soskis MJ, Ho HY, Bloodgood BL, Robichaux MA, Malik AN, Ataman B, Rubin AA, Zieg J,Zhang C, Shokat KM (2012) A chemical genetic approach reveals distinct EphB Signaling mechanisms during brain development. Nat Neurosci 15:1645-1654.

Sperry RW (1963) Chemoaffinity in the orderly growth of nerve fiber patterns and connections Proc. Natl. Acad. Sci. U. S. A., 50:703–710

Stoker AW (2005) Protein tyrosine phosphatases and signaling. J. Endocrinol. 185, 19–33.

Takahashi H, Shintani T, Sakuta H, Noda M (2003) CBF-1 controls the retinotectal topographic map along the anteroposterior axis through multiple mechanisms Development 130: 5203-5215.

Takahashi H, Sakuta H, Shintani T, Noda M (2009) Functional mode of FOXD1/CBF2 for the extablishment of temporal retinal specificity in the developing chick retina. Dev Biol 331: 300-310.

Thakar S, Chenaux G, Henkemeyer M (2011) Critical roles for EphB and ephrin-B bidirectional signalling in retinocollicular mapping. Nat Commun 2:431.

Trapasso F, Drusco A, Costinean S, Alder H, Aqeilan RI, Iuliano R, Gaudio E, Raso C, Zanesi N, Croce CM, Fusco A (2006) Genetic ablation of Ptprj, a mouse cancer susceptibility gene, results in normal growth and development and does not predispose to spontaneous tumorigenesis. DNA Cell Biol 25:376-382.

Tsigankov DN, Koulakov AA (2006) A unifying model for activity-dependent and activity independent mechanisms predict complete structure of topographic maps in ephrin-A deficient mice. J Comput Neurosci 21:101-114.

Van Eekelen M, Overvoorde J, van Rooijen C, den Hertog J (2010) Identification and expression of the family of classical protein-tyrosine phosphatases in zebrafish. PLoS ONE 5(9): e12573.

Van Etten RA, Jackson PK, Baltimore D, Sanders MC, Matsudaira PT, and Janmey PA (1994) The COOH terminus of the c-Abl tyrosine kinase contains distinct F-and G-actin binding domains with bundling activity. J. Cell Biol. 124:325–340.

Wang LC, Dani J, Godement P, Marcus RC, Mason CA (1995) Crossed and uncrossed retinal axons respond differently to cells of the optic chiasm midline in vitro. Neuron 15: 1349-1364.

Williams SE, Mann F, Erskine L, Sakurai T, Wei S, Rossi DJ, Gale NW, Holt CE, Mason CA, Henkemeyer M (2003) Ephrin-B2 and EphB1 mediate retinal axon divergence at the optic chiasm. Neuron 39:919-935.

Wills Z, Bateman J, Korey CA, Comer A, Van Vactor D (1999) The tyrosine kinase Abl and its substrate enabled collaborate with the receptor phosphatase Dlar to control motor axon guidance.Neuron 22:301-312.

Witte ON, Dasgupta A, Baltimore D (1980) Abelson murine leukaemia virus protein is phosphorylated in vitro to form phosphotyrosine. Nature 283: 826–831.

Wilkinson, DG (2000) Topographic mapping: organising by repulsion and competition.

Curr Biol 10:R447-R451.

Woodring PJ, Hunter T, Wang JY (2003) Regulation of F-actin-dependent processes by the Abl family of tyrosine kinases. J Cell Sci 116:2613-2626.

Yang J, Campobasso N, Biju MP, Fisher K, Pan X-Q, Cottom J, Galbraith S, Ho T, et al (2011) Discovery and characterization of a cell-permeable, small-molecule c-Abl kinase activator that binds to the myristoyl binding site. Chem Biol 18:177-186.

Yates PA, Roskies AR, McLaughlin T, O' Leary DDM (2001) Topographic specific axon branching controlled by ephrin-As is the critical event in retinotectal map development. J Neurosci 21:8548-8563.

Yates PA, Holub AD, McLaughlin T, Sejnowski TJ, O'Leary DDM (2004) Computational modeling of retinotopic map development to define contributions of EphA-ephrinA gradients, axon-axon interactions, and patterned activity. J Neurobiol 59:95-113.

Acknowledgments

First and foremost, I would like to thank Professor Masaharu Noda in NIBB for giving me the opportunity to work in such a great scientific environment, for all the valuable suggestions and discussions at various stages of this work.

I greatly thank my supervisor，Associate Professor, Takafumi Shintani in NIBB continuous support of my Ph.D study and continuous encouragement, advice, patient guidance throughout this work.

I would like to thank Mr. Yasushi Takeuchi for teaching me how to perform RGC axons DiI tracing experiments. I thank Mrs. K. Wada and Y. Dokyo for their technical assistance, and Ms. A. Kodama for her secretarial assistance.

I thank Drs. E. Gaudio, F. Trapasso, and A. Fusco for providing me with targeted *Ptprj* heterozygous mice. I thank Dr. T. Shirakawa and RIKEN BRC for providing me with *Ptpro* heterozygous mice.

I thank members of the Model Animal Research Facility of the NIBB Bioresource Center for animal care. I thank the Functional Genomics Facility in NIBB Core Research Facilities for the technical support. This work was supported by grants from the Ministry of Education, Culture, Sports, Science, and Technology of Japan. I would like to thank all the present and past members of the Masaharu Noda's lab for the nice and stimulating working atmosphere.

Finally, I would like to thank my parents and my husband for their mental and financial supports.